

# The role of aerosol in altering North Atlantic atmospheric circulation in winter and impact on air-quality

Francesco S.R. Pausata<sup>1,2\*</sup>, Marco Gaetani<sup>1+</sup>, Gabriele Messori<sup>2</sup>, Silvia Kloster<sup>3</sup>,  
and Frank J. Dentener<sup>1</sup>

## *Affiliation*

<sup>1</sup>*European Commission, Joint Research Centre, Institute for Environment and Sustainability, Ispra (VA), Italy*

<sup>2</sup>*Department of Meteorology, Stockholm University and Bolin Centre for Climate Research, Stockholm, Sweden*

<sup>3</sup>*Land in the Earth System, Max Planck Institute for Meteorology, Hamburg, Germany*

*\*now at Department of Meteorology, Stockholm University and Bolin Centre for Climate Research, 10691, Stockholm, Sweden*

*+now at LATMOS-IPSL, Université Pierre et Marie Curie, Paris, France*

*Corresponding author: francesco.pausata@misu.su.se;*

Numerical model scenarios of future climate depict a global increase in temperatures and changing precipitation patterns, primarily driven by increasing greenhouse gas (GHG) concentrations. Aerosol particles also play an important role by altering the Earth's radiation budget and consequently surface temperature. Here, we use the general circulation aerosol model ECHAM5-HAM, coupled to a mixed layer ocean model, to investigate the impacts of future air pollution mitigation strategies in Europe on winter atmospheric circulation over the North Atlantic. We analyse the extreme case of a maximum feasible end-of-pipe reduction of aerosols in the near future (2030), in combination with increasing GHG concentrations. Our results show a more positive North Atlantic Oscillation (NAO) mean state by 2030, together with a significant eastward shift of the southern centre of action of sea level pressure (SLP). Moreover, we show a significantly increased blocking frequency over the western Mediterranean.

By separating the impacts of aerosols and GHGs, our study suggests that future aerosol abatement may be the primary driver of both the eastward shift in the southern SLP centre of action and the increased blocking frequency over the western Mediterranean. These concomitant modifications of the atmospheric circulation over the Euro-Atlantic sector lead to more stagnant weather conditions that favour air pollutant accumulation especially in the western Mediterranean sector. Changes in atmospheric circulation should therefore be included in future air pollution mitigation assessments. The indicator-based evaluation of atmospheric circulation changes presented in this work will allow an objective first-order assessment of the role of changes in wintertime circulation on future air quality in other climate model simulations.

## 36 1 INTRODUCTION

37 Future climate scenarios indicate a global increase in temperatures and changes in the  
38 hydrological cycle, mainly driven by increasing greenhouse gas (GHG) concentrations (IPCC,  
39 2013). However, GHGs are not the only climate factor responsible for changing the Earth's  
40 radiation budget. Aerosol particles ("aerosols") also play a very important role in altering climate,  
41 both directly – by scattering and absorbing solar radiation – and indirectly – by influencing cloud  
42 radiative properties (cloud albedo effect; Twomey, 1977), and cloud formation and duration (cloud  
43 lifetime effect; Albrecht, 1989). The direct effect of non-absorbing aerosols – such as sulphates –  
44 produces an overall cooling of the atmosphere, while partly absorbing aerosols – such as black and  
45 organic carbon – can lead to either a cooling or a warming, depending on the aerosols' properties  
46 and underlying albedo.

47 Global climate models can realistically reproduce the temperature trend of the last century only  
48 when the radiative impacts of both GHGs and aerosols are included (Gleckler et al., 2008;  
49 Nazarenko and Menon, 2005; Roeckner et al., 1999; IPCC 2013). Therefore, increasing GHG  
50 concentrations as well as changes in aerosol abundance will control future climate and the  
51 associated atmospheric circulation variations. High aerosol concentrations can also have severe  
52 impacts on human health (Lim et al., 2012; WHO, 2013). Consequently, air quality standards have  
53 been introduced in many polluted regions to regulate harmful aerosol concentrations, and the  
54 upward trends in aerosol emissions in the most polluted regions are expected to stabilize or reverse.  
55 Hence, a realistic assessment of on-going and future climate change relies on our ability to predict  
56 trends in both GHG and aerosol emissions, the resulting concentrations and their combined effect  
57 on climate.

58 Most of the GHGs are long-lived and have a geographically homogeneous climate forcing. On  
59 the other hand, aerosol concentrations are highly inhomogeneous, since they are locally controlled  
60 by a combination of primary or precursor emissions, chemical reactions as well as large-scale  
61 atmospheric circulation, and their impacts can have short-term repercussions on climate (Shindell et  
62 al., 2012). Furthermore, atmospheric circulation changes themselves can feedback on air quality.  
63 Modelling and observational analyses suggest that a warming climate degrades air quality, with  
64 increasing surface O<sub>3</sub> and particulate matter abundance in many populated regions (Fiore et al.,  
65 2012). Kloster et al. (2009), for example, used a coupled chemistry-atmosphere general circulation  
66 model to show that climate change alone would worsen the air pollution by aerosols in many world  
67 regions.

68 Several other studies have demonstrated that local-to-regional scale pollutant concentrations  
69 can be influenced by large-scale atmospheric circulation patterns (Eckhardt et al., 2003;  
70 Christoudias et al., 2012; Barnes and Fiore, 2013; Pausata et al., 2012, 2013), such as the North  
71 Atlantic Oscillation (NAO). Pausata et al. (2013) have shown how positive shifts in the NAO in  
72 winter over the North Atlantic penalize cities lying in the Mediterranean area, making it necessary  
73 for these countries to enforce more stringent emission reduction measures. This is of particular  
74 importance in view of a potential shift towards positive NAO regimes under future climate  
75 conditions.

76 The NAO commonly refers to swings in the atmospheric pressure difference between the  
77 subpolar and subtropical North Atlantic, and is the leading mode of winter atmospheric variability  
78 in the North Atlantic. The standard NAO index (NAOI) is defined as the difference in normalized  
79 mean sea-level pressure (SLP) between the Azores (or Portugal) and Iceland (Walker and Bliss,  
80 1932), and determines climate variability from the eastern seaboard of North America to Siberia  
81 and from the Arctic to the subtropical Atlantic. The NAO featured an upward trend of over 1  
82 standard deviation in the 1980s and 1990s compared to the 1951–1970 winter mean (data available  
83 in <http://www.cgd.ucar.edu/staff/jhurrell/naointro.html>). Recent multi-model predictions confirm  
84 previous findings reported in AR4 (e.g., Kuzmina, 2005; Stephenson et al., 2006), of a positive  
85 trend in future winter NAO (Gillett and Fyfe, 2013; Karpechko, 2010). However, there are  
86 substantial variations between NAO projections from different climate models. For example,  
87 Fischer-Bruns et al. (2008) have employed an atmosphere-ocean coupled model (ECHAM4-  
88 OPYC3) and used the Empirical Orthogonal Function (EOF) analysis to investigate future trends in  
89 the NAO. The study found no detectable shift in the leading mode of atmospheric variability under  
90 global warming scenarios. On the other hand, Müller and Roeckner (2008) found a strong positive  
91 trend in the NAO in the ECHAM5/MPI-OM simulations. As a consequence of such uncertainties,  
92 the IPCC AR5, has expressed only medium confidence in near-term projections of NAO changes  
93 (IPCC, 2013).

94 Recently, atmospheric variability in the North Atlantic and the NAO pattern have also been  
95 linked to Rossby wave-breaking in the upper troposphere and to atmospheric blocking (e.g., Croci-  
96 Maspoli et al., 2007; Woollings et al., 2008). The term *atmospheric blocking* is broadly used to  
97 describe situations in which the prevailing westerly flow is blocked, or distorted by a persistent,  
98 quasi-stationary anticyclone (e.g., Rex, 1950; Berrisford et al., 2007). However, the exact  
99 definition varies among studies. For example, Pelly and Hoskins (2003) pioneered the use of  
100 potential vorticity (PV) as an indicator for blocking, linking blocking occurrences to the meridional  
101 potential temperature gradient on a constant PV surface. In this framework, atmospheric blocking is

102 therefore associated with Rossby wave breaking. It has been shown that different blocking patterns  
103 correspond to significantly different large-scale atmospheric circulations over the North Atlantic  
104 basin (Rex, 1950). Blocking situations are often responsible for stagnant atmospheric conditions  
105 that lead to the accumulation of pollutants at ground levels. This increases the likelihood of  
106 exceeding particulate matter (PM) annual and daily limit concentrations, such as those imposed by  
107 European regulations (Directive 2008/50/EC).

108 The aim of this paper is to disentangle the role of future aerosol and GHG concentration changes in  
109 altering atmospheric circulation, expanding earlier analysis that focussed on global scale climate  
110 impacts (Kloster et al., 2009) and the relationship between air pollution mitigation and extreme  
111 events (Kloster et al., 2009; Sillmann et al., 2013). We focus on the extreme case that by 2030  
112 aerosol concentrations will be globally reduced to the maximum feasible extent by using all  
113 presently available end-of-pipe technology, using the results of an aerosol-atmosphere model  
114 coupled with a mixed-layer ocean. Finally, we evaluate the impact of such atmospheric circulation  
115 changes onto PM variability. The analysis includes simulations in which only GHG concentrations,  
116 only aerosol emissions or both are changed. In each simulation the anthropogenic emission  
117 scenarios used to force the model are constant for the entire length of the integration; hence, the  
118 changes in variability depicted by the model will be associated with changes in atmospheric  
119 circulation only. We investigate how GHG and/or aerosol forcings act on: (i) the structure of the  
120 SLP meridional dipole over the North Atlantic in terms of strength and location of its centres of  
121 action; (ii) changes in the NAO in the near future; (iii) the spatial structure and frequency of  
122 atmospheric blocking in the North Atlantic. Finally, we also examine (iv) how future changes in  
123 atmospheric circulation could impact air quality over Europe.

124 This work is structured as follows: Sect. 2 describes the models used, the simulation set-up and  
125 the statistical tools adopted; Sect. 3 presents the GHG and aerosol-induced changes in the  
126 magnitude and spatial pattern of the meridional SLP dipole in the North Atlantic. We also discuss  
127 the related changes in the NAO and atmospheric blocking over the Atlantic, and the effects of such  
128 changes on PM variability. Discussions and conclusions are presented in Sect. 4.

## 129 **2 METHODS**

### 130 **2.1 Climate Model**

131 We have analysed the climate simulations performed by Kloster et al. (2008, 2009) using the  
132 ECHAM5-HAM aerosol-climate model. We focus on the analysis of hitherto unexplored aspects of  
133 atmospheric circulation changes over the North Atlantic. These simulations were also used by  
134 Sillmann et al. (2013) to analyse how changes in precipitation impact on aerosol concentration;

135 however, they focused on annual means and did not consider to what extent these changes were  
136 reflected by large-scale circulation changes that were driving the more localized precipitation  
137 responses.

138 The ECHAM5-HAM modelling system includes the atmospheric general circulation model  
139 ECHAM5 (Roeckner et al., 2003) coupled to a mixed layer ocean (Roeckner et al., 1995), and the  
140 microphysical aerosol model HAM (Stier et al., 2005). The ECHAM5-HAM simulations analysed  
141 in this study (Kloster et al., 2008, 2009) account for both the direct and indirect (cloud lifetime and  
142 cloud albedo effect) aerosol effects. ECHAM5 was run on a T63 horizontal grid (about 1.8° on a  
143 Gaussian Grid), and on 31 vertical levels from the surface up to 10 hPa. A cloud scheme with a  
144 prognostic treatment of cloud droplet and ice crystal number concentration (Lohmann et al., 2007)  
145 provided fractional cloud cover prediction from relative humidity (Sundquist et al., 1989). The  
146 shortwave radiation scheme included 6 bands in the visible and ultraviolet spectra (Cagnazzo et al.,  
147 2007).

148 The microphysical aerosol module HAM treats the aerosol size distribution, mixing state and  
149 composition as prognostic variables. It predicts the evolution of an ensemble of interacting aerosol  
150 modes and is composed of the microphysical core M7 (Vignati, 2004); an emission module for SO<sub>2</sub>,  
151 black and organic carbon, and mineral dust particles; a sulphur oxidation chemistry scheme using  
152 prescribed oxidant concentrations for OH, NO<sub>2</sub>, O<sub>3</sub> and H<sub>2</sub>O<sub>2</sub> (Feichter et al., 1996); a deposition  
153 module; and a module defining the aerosol radiative properties. Prescribing oxidant concentrations,  
154 most importantly H<sub>2</sub>O<sub>2</sub>, may have led to an underestimate in the resulting sulfate burden, since the  
155 use of off-line H<sub>2</sub>O<sub>2</sub> may not accurately account for depletion by aqueous reactions with SO<sub>2</sub> and  
156 recovery in cloud-free conditions. This will increase the gas-phase production of SO<sub>4</sub>, which is less  
157 susceptible to scavenging, and increase the SO<sub>4</sub> burden (Barth et al., 2000; Roelofs et al., 1998).  
158 Another model evaluation of the effect of including explicit oxidation (Pham, 2005) suggested an  
159 overall decline of SO<sub>4</sub> burden (<1 %), but an increase of SO<sub>4</sub> surface concentrations (ca. 5% in  
160 many regions), due to a combination of increased near-surface oxidation and removal processes.  
161 This is a relatively minor error compared to other uncertainties (Textor et al., 2007). The aerosol  
162 optical properties were explicitly simulated using Mie theory and provided as input for the radiation  
163 scheme in ECHAM5 following Toon and Ackerman (1981). Climate-sensitive natural emissions  
164 (dimethyl sulphide, sea salt and dust) were simulated interactively.

## 165 **2.2 Simulation Set-up**

166 The GHG concentrations used in the simulations were derived from the IMAGE 2.2  
167 implementation of the SRES B2 scenario (IMAGE-team, 2001). The SRES B2 storyline describes a

168 world with intermediate population and economic growth, in which the emphasis is on local  
169 solutions to economic, social, and environmental sustainability.

170 The anthropogenic emissions of carbonaceous aerosols, namely black carbon (BC) and organic  
171 carbon (OC), as well as sulphur dioxide (SO<sub>2</sub>), the main precursor of sulphate aerosols, are  
172 extracted from an aerosol emission inventory developed by the International Institute for Applied  
173 System Analysis (IIASA). In this work, a Maximum Feasible Reduction (MFR) air pollutant  
174 emission scenario was explored for the year 2030 (Cofala et al., 2007). MFR assumes the full  
175 implementation of the most advanced available technologies for aerosol emissions abatement. It is  
176 built using projections of human activity levels (industrial production, fuel consumption, livestock  
177 numbers, crop farming, waste treatment and disposal) based on current national perspectives on the  
178 economic and energy development up to the year 2030. In regions where data were not available,  
179 the economic and energy future trends estimated in the IPCC SRES B2 MESSAGE scenario  
180 (Nakicenovic et al., 2000; Riahi and Roehrl, 2000) were considered. Biomass burning emissions,  
181 both anthropogenic and natural, were assumed to stay constant at 2000 levels. Changes in land use  
182 were not taken into account.

183 In the present study the modifications of future North Atlantic atmospheric circulation are  
184 assessed by analysing the differences between near future (year 2030) and present-day (year 2000)  
185 conditions reproduced in climate equilibrium simulations. A 60-yr control simulation was  
186 performed with GHG concentrations, aerosol and aerosol precursor emissions of the year 2000, and  
187 three 30-yr sensitivity equilibrium experiments were performed, using three different combinations  
188 of GHG concentrations and aerosol emissions scenarios:

- 189 • 2000 experiment: year 2000 GHG concentrations and aerosol emissions;
- 190 • 2030 experiment: year 2030 GHG concentrations and MFR aerosol emission scenario;
- 191 • 2030GHG experiment: year 2030 GHG concentrations, and 2000 aerosol emissions;
- 192 • 2030AER experiment: year 2000 GHG concentrations, and 2030 MFR aerosol emission  
193 scenario.

194 All simulation used a spin-up of 30 years, not included in the analysis.

195 The 2030GHG and 2030AER experiments in which, respectively, aerosol emissions and GHG  
196 concentrations remained at the 2000 level, were performed to separate the effects of GHG  
197 concentrations and aerosols emissions. The experimental setups are summarized in Table 1.

### 198 2.3 Statistical analysis methods

199 We evaluate three aspects of the large-scale circulation: 1) the SLP spatial structure (shift of  
200 centres of action); 2) the leading mode of atmospheric variability (NAO); and 3) the blocking  
201 frequency. Finally, we investigate how the atmospheric circulation changes affect PM distributions.

202 To investigate the impact of aerosol and GHG concentration changes on SLP spatial structure,  
203 we define the SLP centres of action for the winter season (January, February and December, DJF)  
204 by creating SLP coherence maps (Pausata et al. 2009). The coherence index value ( $0 \leq CI \leq 1$ ) at each  
205 grid-point is the absolute value of the area-averaged correlation between the monthly SLP time-  
206 series at that point and over the rest of the North Atlantic basin (20°N-85°N; 90°W-40°E). Higher  
207 values indicate that the SLP variability at that location is more *coherent* with variability throughout  
208 the North Atlantic, either in-phase or anti-phase. The Northern and Southern SLP Centres Of Action  
209 (NCOA and SCOA) are identified as CI maxima over the North (north of 55°N) and subtropical  
210 Atlantic (south of 55°N), respectively. This method allows determining the spatial distribution and  
211 shifts of the COAs due to aerosol and GHG concentration changes, both in combination and  
212 separately (for details see Appendix A). In order to verify that the computed geographical shifts in  
213 the centres of action are outside the normal range of inter-annual variability, we use a statistical  
214 bootstrap approach to produce a set of 100 CI maps for the 2000 experiment. We randomly select  
215 subsamples of 20 years for the 30-year long simulations and subsamples of 40 years for the 2000  
216 (60-year long) simulation, and perform the CI analysis for each subsample. Subsequently, we apply  
217 the Student's t-test to determine whether the CI pattern and the shift in the centres of actions  
218 between the 2000 control simulation and the sensitivity studies are significant at 95% confidence  
219 level.

220 Furthermore, in order to assess the variability of the SCOA and evaluate its relation to blocking  
221 frequency and precipitation in the 2000 simulations, we construct an index of the SCOA (SCOAI).  
222 We first generate 10000 random subsamples of 15 years from the 60-year pool of the 2000  
223 simulation. In this case we have reduced the subsample size from 40 to 15 years in order to increase  
224 the variability of the SCOA and hence, better understand its influence on blocking frequency and  
225 precipitation. We then calculate the CI values and determine the position of the SCOA (maximum  
226 in the CI south of 55°N) for each subsample. Hence, we construct the SCOAI where the value of 0  
227 is defined as the 50<sup>th</sup> percentile of the SCOA position within the 10000 subsamples. Eastward  
228 positions (relative to the 50<sup>th</sup> percentile) of the SCOA are defined as positive values of the SCOAI  
229 and westward position as negative ones. The SCOAI has then been normalized by the standard  
230 deviations of the eastward and westward SCOA positions.

231 Winter changes in the leading mode of atmospheric variability are investigated by using the  
 232 monthly NAO Index (NAOI), defined as the difference in the normalized SLP anomalies between  
 233 Ponte Delgada, Azores, and Stykkisholmur/Reykjavik, Iceland. The NAOI allows to look for shifts  
 234 in the North Atlantic atmospheric circulation associated with future climate change (Hurrell, 1995).

235 The analysis of blocking frequency over the North Atlantic basin is performed as follows. In  
 236 order to define atmospheric blocking, the present paper utilizes a bi-dimensional index that  
 237 identifies reversals in the meridional gradient of 500 hPa geopotential height (Davini and Cagnazzo,  
 238 2013; Davini et al., 2012; Tibaldi and Molteni, 1990). For every model gridbox with coordinates  
 239 (*latitude* =  $\varphi$ , *longitude* =  $\lambda$ ), the following two quantities are defined:

$$240 \quad \Delta_N(\varphi, \lambda) = \frac{Z_{500}(\varphi, \lambda) - Z_{500}(\varphi - 15^\circ, \lambda)}{15^\circ},$$

$$241 \quad \Delta_S(\varphi, \lambda) = \frac{Z_{500}(\varphi + 15^\circ, \lambda) - Z_{500}(\varphi, \lambda)}{15^\circ},$$

242 over the domain where  $30^\circ N < \varphi < 72.5^\circ N$ ,  $180^\circ W < \lambda \leq 180^\circ E$ . In order for a gridbox to be  
 243 flagged as ‘blocked’, the following must hold:

$$\Delta_N > 0; \Delta_S < -10 \text{ m}/^\circ \text{ latitude}$$

244 In order to define a blocking event, a number of additional constraints are also enforced.  
 245 Firstly, a cluster of adjacent blocked gridboxes spanning at least  $15^\circ$  longitude must be identified at  
 246 a given timestep. Therefore, if a gridbox is blocked in isolation, it is not considered to be part of a  
 247 blocking event. A persistence criterion is also applied: a blocking event requires that at least another  
 248 blocked gridbox is detected for 5 consecutive days within an area of  $5^\circ$  latitude by  $10^\circ$  longitude,  
 249 centred on the original blocked gridbox.

250 The impacts of changes in atmospheric circulation on air pollution are investigated by  
 251 analysing changes in PM monthly anomaly distributions. We focus on changes in the skewness of  
 252 distributions for the winter season. The skewness is the distribution’s third standardized moment,  
 253 and is a measure of the asymmetry of the distribution. Positive skewness values typically indicate  
 254 that the right side tail of the distribution becomes longer than the left side, and vice-versa for  
 255 negative values. Significance in the skewness differences is assessed by using a Kolmogorov-  
 256 Smirnov test at 95% confidence level. This test is a non-parametric tool, meaning that it makes no  
 257 assumptions on the shape of the data distribution. An ‘artificial’ variability is introduced in the  
 258 skewness values in each simulation through a bootstrap technique. For each experiment, we  
 259 calculate the skewness values of 100 random distributions, generated from the original pool of 30 or  
 260 60 years using the same bootstrap technique described for the CI. The significance level is then  
 261 identified based on this sample.



## 262 3 RESULTS

263 The results presented here describe the effects of GHG and aerosol concentrations on the mean  
264 state and variability of the North Atlantic atmospheric circulation. The results are presented in three  
265 sections. In the first section, changes in the spatial structure of the SLP and its variability are  
266 investigated. In the second section, we extend the analysis to changes in the blocking frequency.  
267 Finally, in the third section, we quantify the impacts of such changes on precipitation regime and  
268 PM variability.

### 269 3.1 Changes in SLP centres of action and their variability

270 The 2030 and 2030AER simulations show a north-eastward shift of the SCOA compared to the  
271 2000 control simulation (Fig. 1). The area of highest SLP coherence in the 2000 simulation is  
272 located in the central-western part of the sub-tropical North Atlantic, whereas in the 2030  
273 simulation it is shifted off the coast of northern Morocco. The NCOA, instead, remains located in  
274 central western Greenland for all scenarios. However, in the 2030 and 2030AER simulations, a  
275 secondary CI maximum develops in the Norwegian Sea, and the areas with the CI maxima are  
276 broader. Secondary CI maxima also develop at low latitudes compared to the 2000 simulation (Fig.  
277 1).

278 Both sensitivity simulations (2030GHG and 2030AER) show a significant north-eastward shift  
279 (see section 2.3) of the SCOA as well as broader areas of CI maxima compared to the 2000  
280 simulation. Both these features are more pronounced in the 2030AER than in the 2030GHG  
281 simulation, in particular the displacement towards the Mediterranean Sea of the SCOA.

282 With regard to the SLP variability, the 2030 simulation shows a significant positive shift of the  
283 NAO mean state by 0.46 compared to the 2000 control period (Fig. 2). The probability of having an  
284 NAOI greater than +1 increases from 30% to 40% (Fig. 2). Neither the GHG increase (2030GHG)  
285 nor the aerosol reduction (2030AER) have any statistically significant role in changing the NAO  
286 mean state and the frequency distribution of strongly positive/negative NAO phases relative to the  
287 control simulation. *Nevertheless, the GHG increase shows a higher probability to contribute to*  
288 *the NAO shift compared to aerosol alone: in the 2030AER simulation the likelihood is at 65%,*  
289 *while in 2030GHG simulation is at 85% confidence level (using a t-test).* Only the combination of  
290 both 2030 GHGs and aerosol emissions leads to a statistically significant change in the NAO mean  
291 state at 95% confidence level.

292 Hence, whereas the NAO shift is related to both aerosol and GHG changes (with likely stronger  
293 impacts from the GHGs), the aerosol reduction alone plays the largest role in shifting the southern  
294 centre of action of SLP towards the Mediterranean.

## 295 **3.2 Changes in blocking frequency**

296 Blocking events can have a large impact on weather patterns and sometimes lead to the  
297 occurrence of extreme events (e.g., Yiou and Nogaj, 2004); hence, it is important to quantify the  
298 variability and possible changes in the preferred location of blocking occurrences.

299 The 2000 simulation shows a blocking frequency that peaks in the south over the sub-tropical  
300 North Atlantic (low-latitude blocking, LLB) and in the north over Greenland (high-latitude  
301 blocking, HLB), as shown in Figure 3a. The LLB events are linked to a northward displacement of  
302 the subtropical high-pressure system. The HLB events are characterized by long durations (on the  
303 order of 9 days), diverting the main flow southward (Davini et al., 2012). The simulated 2000  
304 blocking climatology is slightly different from the patterns seen in re-analysis data, which have a  
305 higher activity over the Nordic seas, but nevertheless shows a strong resemblance to the observed  
306 climatology (cf. Fig. 3a with Fig. 1 in Davini et al., 2012a).

307 HLBs and LLBs are strongly tied to the phase of the NAO: Woollings et al. (2008) showed that  
308 HLB events over Greenland are strongly anti-correlated with the NAOI. Furthermore, changes in  
309 the HLB position (Wang and Magnusdottir, 2012) and frequency (Davini et al., 2012b) have been  
310 shown to influence not only the NAOI, but also its pattern. Yao and Luo (2014) have described the  
311 relationship between HLBs and LLBs and the NAO phase in winter during the period 1950-2011.  
312 The HLBs are connected not only to the NAO phase but also to the position of the SCOA. By  
313 regressing the NAOI and the SCOA time-series onto the blocking frequency field in the 2000  
314 simulation (see details in Appendix B), we analyze how the NAO phase and the position of the  
315 SCOA affect the blocking frequency. Positive NAO phases are associated to a northward increase  
316 of LLBs (Fig. 4a), whereas eastward positions of the SCOA are connected to a northeastward  
317 increase of LLBs (Fig. 4b). The regression analysis also shows a decreased HLB frequency over  
318 Greenland during positive NAO phases in agreement with the above-mentioned studies.

319 The 2030 simulation shows a significant increase (up to 50-70%) in the number of LLB events  
320 over western Europe and the Mediterranean basin, corresponding to a more invasive subtropical  
321 anticyclone (high-pressure system) over southern and central Europe in winter. The increased LLB  
322 frequency in the 2030 simulation is consistent with both a positive NAO shift (Fig. 4a) and an  
323 eastward shift of the SCOA (Fig. 4b). On the other hand, HLBs decrease (Fig. 3b) is in agreement  
324 with the reduction in negative NAO phases discussed in Section 3.1 and the NAOI-blocking  
325 frequency relationship highlighted in figure 4a.

326 The 2030GHG and 2030AER simulations also show significant increases in the LLB frequency  
327 over the mid-latitude North Atlantic and decreases in the HLB frequency (Fig. 3c and 3d).  
328 However, the patterns are different from one another: the high-latitude change in both 2030GHG

329 and 2030 closely approximates the blocking frequency difference between the positive and negative  
330 phases of the NAO, shown in figure 4a (cf. with figure 3b and 3c). On the other hand, the HLB  
331 frequency change in the 2030AER experiment seems to be related to a shift in the SCOA (cf. 3d  
332 and 4b). This is consistent with the large (small) eastward displacement of the SCOA in the  
333 2030AER (2030GHG) simulation and the smaller (larger) shift in the NAO mean state.

334 The 2030AER simulation also shows a significant increase in LLB frequency over the  
335 Mediterranean, not seen in the 2030GHG experiment. Hence, the aerosol concentration reduction  
336 seems to be the main driver of the increase in LLB events over the Mediterranean seen in the 2030  
337 simulation (Fig. 3 cf. panels b and d). These results strengthen the role of aerosols in affecting  
338 atmospheric dynamics in the North Atlantic, suggesting that they drive both a) an eastward shift of  
339 the southern centre of action of SLP and b) an increased tendency of the sub-tropical anticyclone to  
340 expand towards the Mediterranean Sea.

### 341 **3.3 Impacts on air-quality**

342 Large-scale changes in atmospheric circulation can affect PM variability over Europe by  
343 altering the precipitation regime. The latter is one of the main mechanisms for PM removal, and  
344 affects PM concentrations at the surface (e.g., Horton et al., 2014; Jacob and Winner, 2009; Pausata  
345 et al., 2013). For example, an eastward shift of the SCOA and/or a shift towards positive NAOI,  
346 together with an increased frequency of blocking events in the Mediterranean, may lead to a higher  
347 frequency of dry, stagnant weather conditions in south-western Europe, thus worsening air quality  
348 (see Appendix C for a discussion on the relationship between circulation changes and precipitation).  
349 Hence, even though there will be an overall improvement in air quality conditions associated with  
350 an abatement of PM emissions, additional PM emission reduction measures may be necessary for  
351 those countries and cities lying in the Mediterranean area to counterbalance the effects of the  
352 atmospheric circulation changes. This hypothesis has already been suggested by Pausata et al.  
353 (2013) on the basis of an NAO-PM analysis using the same model driven by ERA-40 re-analysis  
354 data. In this work, we test it further by analyzing climate sensitivity experiments under different  
355 aerosol emission scenarios for the near future. We aim to provide a general coherent overview of  
356 the impacts of large-scale circulation changes on air-quality. We focus on monthly PM data, similar  
357 to the monthly SLP field used for the NAOI and CI analyses. We do not discuss the daily  
358 exceedances of EU thresholds, since this would be beyond the scope of the present study, and the  
359 coarse resolution global model has limited skills on simulating them (Pausata et al., 2013).

360 To quantify how the changes in atmospheric circulation affect air-quality, we calculate the  
361 relative anomaly distributions of PM concentrations for four regions (see also figure 3a), to  
362 encompass the different areas of influence of the NAO over Europe:

- 363 • Western Mediterranean (WM): 34°N-43°N / 0°-10°W;
- 364 • Eastern Mediterranean (EM): 34°N-43°N / 10°E-40°E;
- 365 • Central Europe (CE): 44°N-53°N / 0°-15°E;
- 366 • Eastern Europe (EE): 46°N-60°N / 20°E-40°E.

367 In the PM we have considered only the aerosol components included in ECHAM5-HAM that  
368 have a predominantly anthropogenic signature – namely black and organic carbon, and sulphates –  
369 disregarding aerosols of natural origin (e.g., sea-salt, mineral dust). Thus, the PM in this paper  
370 represents mostly PM<sub>2.5</sub>, and is likely a lower bound on the ‘real’ PM concentrations (for an  
371 evaluation of correspondence between modelled and measured PM<sub>2.5</sub>/PM<sub>10</sub> see the Supplementary  
372 Material in Pausata et al., 2013).

373 First, we analyse the skewnesses of the monthly PM relative anomaly distributions for the  
374 winter season. PM relative anomaly distributions for all experiments and for all four regions show  
375 positive skewness values, meaning that positive PM anomalies are becoming more likely than  
376 negative ones (Fig. 5 and Table 2). Our results show that, in all three 2030 experiments, the  
377 simulated PM distributions change significantly in all regions considered due to the altered  
378 atmospheric circulation (Fig. 5 and Table 2).

379 In the Western Mediterranean (WM), the PM relative anomaly skewness increases remarkably  
380 from 0.26 in the 2000 case to 1.02 and 1.05 in the 2030 and 2030AER simulations, respectively.  
381 This change is mainly led by the aerosol reduction, whereas the GHGs only drive a small  
382 contribution (Table 2). The large change in skewness in the 2030 simulation is accompanied by a  
383 corresponding shift in the upper and lower percentiles of the distribution. The 5<sup>th</sup> and 95<sup>th</sup>  
384 percentiles rise by 8% and 4% respectively relative to 2000, indicating a transition towards more  
385 positive PM anomalies (Table 3). The rise in PM extremes matches the changes in rainy day  
386 extreme percentiles (not shown). The 95<sup>th</sup> and 5<sup>th</sup> percentiles of the frequency of rainy days  
387 decrease by 2% and 17% respectively. Rainy day frequencies and PM anomalies are anti-correlated;  
388 therefore, a change in the 95<sup>th</sup> (5<sup>th</sup>) percentile in rainy days should be associated with a change of  
389 the opposite sign in the 5<sup>th</sup> (95<sup>th</sup>) percentile in the PM anomalies.

390 The Eastern Mediterranean (EM) also experiences an increased skewness in the 2030  
391 simulation relative to 2000. However, the changes are smaller compared to the WM, possibly  
392 because of the greater distance from the SCOAA – located off the coast of the Iberian Peninsula in  
393 the 2030 simulation – and the contrasting effect of the NAO phase inside the domain: as one moves  
394 further to the east in the Mediterranean basin, the correlation between NAO and precipitation  
395 changes sign (Fig. B1a). The smaller changes in the PM distribution simulated in the EM compared

396 to the WM could therefore be related to a different behaviour in precipitation regime (see Appendix  
397 B).

398 On the other hand, Central (CE) and Eastern Europe (EE) show a decreased skewness in the 2030  
399 case compared to the 2000 simulation. CE displays a shift in skewness from 1.44 to 0.66; the  
400 corresponding shift in EE is from 1.70 to 1.18. Furthermore, CE also shows an increment in the  
401 number of negative extremes, with a 14% decrease in the 5<sup>th</sup> percentile. However, CE also  
402 experiences an increase in positive extremes with a +7% shift in the 95<sup>th</sup> percentile in the 2030  
403 simulation compared to the 2000 experiment (Table 3). The change in the extreme PM percentiles is  
404 accompanied by a similar but opposite change in the rainy day percentiles: +3% and -9% for the  
405 95<sup>th</sup> and 5<sup>th</sup> percentiles, respectively. CE is located closer to the transition area of the NAO  
406 influence between northern Europe and Mediterranean basin (see also figure B1). Therefore, this  
407 area may be exposed to alternation of a more invasive Azores high and rainy Atlantic storms.  
408

409 Therefore, the regions that will be most affected by future large-scale circulation changes are  
410 the Western Mediterranean and Central Europe, both with increased high PM concentration  
411 episodes, but the latter also with a strong increment in low PM values relative to 2000. The  
412 implications of these results for air quality policy are discussed in the following section.

#### 413 **4 Discussions and Conclusions**

414 The present study analyses future scenarios of atmospheric circulation over the North Atlantic  
415 and possible impacts on air quality over Europe. The chemistry-atmosphere ECHAM5-HAM  
416 model, coupled to a mixed layer ocean, shows a change towards more positive NAO phases,  
417 together with an eastward shift of the southern SLP centre of action. These shifts are associated to  
418 an increased frequency of blocking events over the western Mediterranean. Our results highlight  
419 how the decreased aerosol and aerosol precursor emissions, along with GHGs, are responsible for  
420 changes in radiative forcing that feedback onto the atmospheric circulation and alter the NAO mean  
421 state. Table 4 provides a qualitative summary of the atmospheric changes induced by 2030 GHGs,  
422 aerosols and jointly by GHG and aerosol emissions on a variety of circulation indicators. These  
423 changes in atmospheric circulation in turn feedback significantly on air quality, and would lead to  
424 an increase in the magnitude of extreme pollution events over the western Mediterranean if no  
425 changes in aerosol emissions were observed. In the MFR scenario analysed in our study, however,  
426 the reduction in aerosol emissions would outstand the increase in PM extreme values leading to an  
427 overall improvement of air quality.

428 Future shifts in the NAO phase have already been discussed by several modelling studies (e.g.,  
429 Gillett and Fyfe, 2013; Karpechko, 2010; Stephenson et al., 2006; Kuzmina, 2005; Hu and Wu,

430 2004); however, the driving mechanisms behind these shifts are still debated. Hori et al. (2007)  
431 have shown that NAO variability does not change substantially in the SRES-A1B scenarios  
432 compared to the 20th century, and conclude that the trend in the NAO index is the result of an  
433 anthropogenic trend in the basic mean state, rather than being due to changes in NAO variability.  
434 Our results support Hori et al.'s (2007) findings by showing that anthropogenic changes in GHG  
435 and aerosols lead to a change in the NAO's mean state rather than its variability (Fig. 2).

436 The positive NAO shift comes along with a shift of the SLP centres of action. Hilmer and Jung  
437 (2000) have found an eastward shift in the SLP pattern associated with the inter-annual variability  
438 of the NAO from 1958-1977 to 1978-1997. Peterson et al. (2003) have suggested that this shift is  
439 simply a consequence of the trend towards a more positive NAO index in the last two decades of  
440 the 20<sup>th</sup> century. Hu and Wu (2004), using both data and a coupled general circulation model, have  
441 also shown that a shift of both SLP centres of action took place in the second half of the last  
442 century, which will likely continue in the future. Our study confirms that this shift also occurs under  
443 a global warming scenario. However, while in our simulations the southern centre undergoes a  
444 remarkable eastward shift, the northern one is fairly stable around southern Greenland – as  
445 demonstrated using the coherence index approach (Fig. 1). Nevertheless, the CI maps do show that  
446 in the 2030 simulations a secondary northern maximum – not present in the 2000 experiment –  
447 appears in the Norwegian Sea (Fig. 1). Furthermore, our simulations highlight how the future  
448 abatement of the aerosol load may play an important role in the eastward shift of the SLP centres of  
449 action.

450 The present study also finds an increased blocking frequency over the western Mediterranean.  
451 Such increase, together with an eastward displacement of the southern SLP centre of action and a  
452 positive shift of the NAO mean state, leads to more frequent stagnant weather conditions that favour  
453 pollutant accumulation in the Mediterranean. This change in frequency of pollution events has also  
454 been described by Kloster et al. (2009), who showed that aerosol abundance is dependent on the  
455 climate state, as also highlighted in a number of other modelling studies (e.g., Feichter et al., 2004;  
456 and overview in IPCC, 2013). Kloster et al. (2009) further found that aerosol burdens increase in  
457 the area due to less precipitation and reduced wet-deposition. Hence, they suggest that climate  
458 change alone would worsen air pollution by aerosols. Here we show that in Europe these findings  
459 are consistent with a straightforward NAO-behaviour analysis. A positive shift in future NAO  
460 would indeed lead to more intense extreme pollution events over specific areas, such as the western  
461 Mediterranean countries, assuming constant present-day aerosol emissions. This result also supports  
462 the hypothesis of Pausata et al. (2013) that - for aerosol emissions fixed at present day values –  
463 climate change would lead to more extreme pollution events over the western Mediterranean,

464 forcing southern European countries to implement more stringent abatement measures to counteract  
465 adverse changes in PM variability. However, our study also highlights that the increase in the  
466 number of high PM episodes in the western Mediterranean is partially counterbalanced by a lower  
467 median and a narrowing of the PM frequency distribution around the median itself (Fig. 5 and Table  
468 3).

469 Current European legislation considers PM air quality thresholds of  $25 \mu\text{g}/\text{m}^3$  (annual average)  
470 for  $\text{PM}_{2.5}$ , and  $50 \mu\text{g}/\text{m}^3$  for  $\text{PM}_{10}$  (24 hours, not to be exceeded for more than 35 days per year).  
471 European legislation has also set an indicative target value for  $\text{PM}_{2.5}$  annual average of  $20 \mu\text{g}/\text{m}^3$ .  
472 Currently, between 20-31% and 22-33% of the urban population in Europe is exposed to  $\text{PM}_{2.5}$   
473 levels above the  $20 \mu\text{g}/\text{m}^3$  threshold (EEA, 2013). However, more stringent standards are currently  
474 in place in the USA (annual  $\text{PM}_{2.5}$ :  $12 \mu\text{g}/\text{m}^3$ ), or recommended by the World Health Organization –  
475 WHO (annual  $\text{PM}_{2.5}/\text{PM}_{10}$ :  $10/20 \mu\text{g}/\text{m}^3$ ), and may be adopted in Europe as well at some point in  
476 the future. Considering the more stringent WHO guidelines, currently between 91-96% ( $\text{PM}_{2.5}$ ) and  
477 85-88% ( $\text{PM}_{10}$ ) of urban population is exposed to values above the thresholds  
478 (<http://ec.europa.eu/environment/air/quality/standards.htm>). Depending on threshold levels set by  
479 future EU air quality legislation, it is not *a-priori* clear how changes in PM frequency distributions  
480 will affect exceedance of these thresholds, and what levels of emission reductions are appropriate to  
481 reach these air quality objectives.

482 Unfortunately, our coarse resolution global model results only allow a qualitative assessment of  
483 the impact on air quality exceedance of future air pollution emissions and climate change.  
484 Therefore, we envision the need for more in-depth studies to further quantify the significance of our  
485 findings with respect to the relationship between future changes in atmospheric circulation and air-  
486 quality related issues. These studies should make use of both high vertically resolved coupled  
487 atmosphere-ocean general circulation models and regional air-quality models. The former models  
488 are needed to better quantify anthropogenic-induced changes in atmospheric circulation and their  
489 impacts on air quality, given the strong coupling between stratospheric and tropospheric circulation  
490 (e.g., Hoerling et al., 2001; Scaife et al., 2005; Omrani et al., 2013). The latter models can better  
491 constrain the effects of the altered atmospheric circulation on air-quality at regional scales. The  
492 aerosol 2030 simulations used in this study assumed the MFR scenario; the extent to which these  
493 maximum-feasible air pollutant emission reductions will actually happen depends on the  
494 effectiveness of policies. Nevertheless, 60-70% of the reduction (compared to a 2000 baseline)  
495 assumed by the MFR scenario is not unrealistic and hence some of the feedbacks seen in this study  
496 are likely to be witnessed in the real world. Most of the EU estimates of benefits related to pollution  
497 reduction (e.g., a decrease in the number of premature deaths) are determined without taking into

498 account the potential effect of a future atmospheric circulation changes. Therefore, more  
499 quantitative studies in which high-resolution regional air quality models are coupled to global  
500 ocean-atmosphere-chemistry climate models are necessary to assess the climate feedbacks on  
501 aerosol abatement. Understanding and characterizing changes in the NAO in global models, thus,  
502 providing meteorological and chemical boundary conditions for regional air quality models, will  
503 also allow for a better analysis of exceedance rates of air quality standards associated with the inter-  
504 annual variability of circulation patterns.

### 505 *Appendix A*

506 In Appendix A we explain in detail the relationship between the coherence index (CI) analysis  
507 and the NAO. The CI analysis of the SLP field identifies the areas that best correlate with the SLP  
508 variability over a given basin. In other words, the maxima in the CI represent the points that best  
509 capture SLP variability within a given domain. On the other hand, the NAOI is a measure of the  
510 wintertime SLP swings between two specific points in the North Atlantic, located in the "eye" of  
511 the two stable pressure areas, the Azores high and Icelandic low. Therefore, these two locations  
512 capture a substantial amount of SLP variability in the basin. Pausata et al. (2009) have already  
513 shown how the CI and the NAOI are connected to each other in the present climate. The CI patterns  
514 of surface temperature (precipitation) closely resemble the correlation patterns between surface  
515 temperature (precipitation) and the leading Principal Component (PC1) of the SLP field (which is  
516 an alternative definition of the NAOI; see figures 7 and 8 in Pausata et al., 2009). To further  
517 demonstrate the link between the CI and NAOI, we have calculated the correlation between SLP  
518 and the leading PC of the SLP field, following Pausata et al. (2009). For simplicity, in the  
519 manuscript we have used the canonical definition of the NAOI, since the PC1 and NAOI in winter  
520 are highly correlated ( $r > 0.90$ , see also Hurrell, 1995). Figure A1 shows that the correlation  
521 between the PC1 and SLP is very similar to the CI pattern and the correlation maxima of both  
522 analyses are quite close to each other (cf. Figs A1 and 1a). The advantage of the CI analysis  
523 compared to the PC/SLP (or temperature or precipitation) correlation analysis is that the CI analysis  
524 does not depend only on the leading mode of variability but directly integrates all other modes that  
525 directly affect the fluctuations of the analyzed variable.

526 Pausata et al. (2009) have also shown that, during different climate states in which the leading  
527 mode of SLP variability (PC1) is less dominant (lower explained variability of the EOF1), the CI  
528 and the PC correlation patterns can be completely different. Therefore, we have decided to adopt  
529 the CI in addition to the canonical NAOI as a further metric to better understand and interpret large-  
530 scale circulation changes.

531



532  
533  
534  
535  
536  
537  
538  
539  
540  
541  
542  
543  
544  
545  
546  
547  
548  
549  
550  
551  
552

### *Appendix B*

In Appendix B, we examine how the large-scale atmospheric indicators used in this study are related to the number of rainy days in DJF over Europe. PM concentrations at the surface can be affected by different factors such as precipitation or the thermal structure of the boundary layer. However, these factors are implicitly included in the large-scale changes in atmospheric circulation, i.e. the changes in the CI pattern, NAO phase and blocking events.

We focus on the average number of rainy days per month during winter, because the monthly aerosol concentrations are more strongly affected by the number of rainy days (even with small precipitation amounts) rather than by the total intensity of the monthly precipitation (Claassen and Halm, 1995). We define a rainy day as a day with precipitation > 1 mm at a given grid-box.

In order to study the degree to which rainy day anomalies are associated to the NAO phase and the position of the southern SLP centre of action (SCOA) in the 2000 simulation, we use a regression analysis: a regression coefficient  $b(i,j)$  is calculated at each specific latitude ( $i$ ) and longitude ( $j$ ) by linearly regressing the input variable of interest (e.g., rainy days( $t,i,j$ ), blocking frequency anomalies) against the reference time series (e.g., NAOI( $t$ ) or SCOA Index – SCOAI( $t$ )).

The corresponding regression map is a composite field consisting of a linear combination of all available data, where each datum (e.g., rainy day/blocking frequency anomaly) is weighted by the concurrent value of the index (e.g., NAOI/SCOAI) time series:

$$b(i,j) = \left(\frac{1}{N}\right) \times \sum_{t=1}^N [\text{Rday}^{\text{anom}}(t,i,j) \times \text{INDEX}(t)],$$

553  
554 where  $N$  is the number of time samples. The  $b(i,j)$  coefficients may be viewed as the  
555 perturbations in rainy day frequency at the  $(i,j)^{\text{th}}$  grid point observed in association with a positive  
556 perturbation in the INDEX( $t$ ) (NAOI( $t$ ) or SCOAI( $t$ ) by one standard deviation (i.e. NAOI/SCOAI  
557 = 1) (Lim and Wallace, 1991). For simplicity, we only show the anomalies associated with positive  
558 NAO (SCOA) phases; by construction, the anomaly pattern associated with the negative NAO  
559 phase differs only in sign. The regressions of the NAOI and SCOAI clearly show the influence of  
560 both the NAO phase and the position of the SCOA on rainy day frequency (Fig. B1). Positive NAO  
561 phases and SCOAs shifted to the east lead to decreased numbers of rainy days over the central-  
562 western Mediterranean and increases over part of central Europe. The opposite influence is found

563 for the eastern Mediterranean, where a positive NAO phase is associated to an increased number of  
564 rainy days, while an eastward location of the southern SLP maximum is linked to a decreased  
565 number of rainy days.

566 Finally, we related rainy day anomalies in each of the four selected regions in Europe (WM, EM,  
567 CE and EE) to the frequency of blocking events in the Atlantic sector ( $30^{\circ}$ – $72^{\circ}$ N,  $80^{\circ}$ W– $45^{\circ}$ E). To  
568 do so, we have constructed a composite map for each domain. We take each gridpoint ( $X_{fd}$ ,  $Y_{fd}$ )  
569 within the full domain (entire Atlantic sector), and compute the frequency in rainy days at each  
570 gridpoint ( $x_{rd}$ ,  $y_{rd}$ ) within the regional domain (WM, EM, CE or EE) while gridpoint ( $X_{fd}$ ,  $Y_{fd}$ ) is  
571 blocked. Such values are assigned to gridpoint ( $X_{fd}$ ,  $Y_{fd}$ ). This calculation is then repeated for days  
572 on which gridpoint ( $X_{fd}$ ,  $Y_{fd}$ ) is unblocked. An anomaly in frequency of rainy days between the  
573 blocked and unblocked cases is then found. This means that, for each gridpoint ( $X_{fd}$ ,  $Y_{fd}$ ) in the full  
574 domain, we have several percentage anomalies, one for each gridpoint ( $x_{rd}$ ,  $y_{rd}$ ) within the regional  
575 domain. To obtain the composite map for each regional domain, we then average these values to  
576 obtain a single percentage value for each gridpoint ( $X_{fd}$ ,  $Y_{fd}$ ). For example, for WM the positive  
577 values over southern Norway indicate that, when there is a blocking event over this area, an  
578 increase in rainy days by about 10% is expected over the WM compared to the case with no  
579 blocking over southern Norway. The value of 10% is an average over the response at each of the  
580 gridpoints ( $x_{rd}$ ,  $y_{rd}$ ) within the WM domain. On the other hand, blocking events to the west of and  
581 over the WM lead to a 10-15% increase in rainy days relative to the case with no blocking events  
582 over the same regions (Fig. B2a).

583 Hence, our analysis shows, as expected, that increased numbers of blocking events over western  
584 Europe and the eastern North Atlantic are associated with reduced numbers of rainy days over the  
585 Iberian Peninsula, while high-latitude blockings are associated with more precipitation days over  
586 the WM (Fig. B2a). For the EM, on the opposite, the blocking frequency over western Europe and  
587 the eastern North Atlantic does not have a remarkable influence (Fig. B2c). This, together with a  
588 contrasting influence on this region of the NAO and SCOA shifts (Fig. B1) may be responsible for  
589 the sometimes apparently ambiguous change in PM anomalies simulated in the three 2030  
590 experiments.

591 This analysis shows how rainy days are connected to the large-scale circulation patterns  
592 investigated in this study, providing a context for their impact on PM concentrations at the surface.

593

594

595

597 In Appendix C, we examine how the number of rainy days in DJF changes in the 2030  
598 simulations compared to the 2000 control experiment over Europe. This step will provide a better  
599 understanding on how the atmospheric circulation changes may impact – through changes in the  
600 number of rainy-days – PM distributions in the future.

601 The 2030 simulation shows a clear dipole pattern, with an increased number of rainy days (up  
602 to 60%) in central-northern Europe and a reduction (up to 50%) in southern Europe, relative to 2000  
603 simulation (Fig. C1). In general, similar patterns are found in the 2030GHG and 2030AER cases.  
604 However, there are some remarkable differences over the British Isles, central Europe and southern  
605 Norway, as well as the Mediterranean basin. The increase in rainy days in the 2030AER seems to  
606 be shifted further south compared to 2030GHG, leading to more rainy days over the British Isles  
607 and central Europe (2030AER) instead of the northern North Atlantic and Southern Norway  
608 (2030GHG). The 2030AER simulation further shows a significant decrease in rainy days confined  
609 to the central-western part of the Mediterranean and to the southern North Atlantic, whereas in the  
610 2030GHG the decrease is spread out over the entire Mediterranean. The combination of the  
611 2030GHG and 2030AER changes in rainy days resembles the 2030 anomaly pattern (Fig. C1). The  
612 difference between the 2030GHG and 2030AER anomalies is likely related to the different changes  
613 in atmospheric circulations discussed in Sections 3.1 and 3.2. The 2030GHG case experiences a  
614 more pronounced shift in the NAO phase compared to the 2030AER simulation and no changes in  
615 the SCOA. The 2030AER, on the other hand, is characterized by a significant eastward shift of the  
616 SCOA but only a small shift in the NAO (see appendix B).

#### 617 Acknowledgements

618 FSR Pausata and FJ Dentener were funded by the EU FP7 project PEGASOS. The authors would like to  
619 thank P. Davini for discussions and suggestions on the atmospheric blocking analysis, and the two  
620 anonymous reviewers.

#### 621 References

622 Albrecht, B. A.: Aerosols, cloud microphysics, and fractional cloudiness., *Science*, 245(4923),  
623 1227–30, doi:10.1126/science.245.4923.1227, 1989.

624 Barnes, E. A. and Fiore, A. M.: Surface ozone variability and the jet position: Implications for  
625 projecting future air quality, *Geophys. Res. Lett.*, 40(11), 2839–2844, doi:10.1002/grl.50411, 2013.

626 Barth, M. C., Rasch, P. J., Kiehl, J. T., Benkovitz, C. M. and Schwartz, S. E.: Sulfur chemistry  
627 in the National Center for Atmospheric Research Community Climate Model: Description,  
628 evaluation, features, and sensitivity to aqueous chemistry, *J. Geophys. Res.*, 105(D1), 1387,  
629 doi:10.1029/1999JD900773, 2000.

630 Berrisford, P., Hoskins, B. J. and Tyrlis, E.: Blocking and Rossby Wave Breaking on the  
631 Dynamical Tropopause in the Southern Hemisphere, *J. Atmos. Sci.*, 64(8), 2881–2898,  
632 doi:10.1175/JAS3984.1, 2007.

633 Cagnazzo, C., Manzini, E., Giorgetta, M. A., Forster, P. M. D. F. and Morcrette, J. J.: Impact of  
634 an improved shortwave radiation scheme in the MAECHAM5 General Circulation Model, *Atmos.*  
635 *Chem. Phys.*, 7(10), 2503–2515, doi:10.5194/acp-7-2503-2007, 2007.

636 Christoudias, T., Pozzer, A. and Lelieveld, J.: Influence of the North Atlantic Oscillation on air  
637 pollution transport, *Atmos. Chem. Phys.*, 12(2), 869–877, doi:10.5194/acp-12-869-2012, 2012.

638 Claassen, H. C. and Halm, D. R.: A possible deficiency in estimates of wet deposition obtained  
639 from data generated by the NADP/NTN network, *Atmos. Environ.*, 29(3), 437–448,  
640 doi:10.1016/1352-2310(94)00182-K, 1995.

641 Cofala, J., Amann, M., Klimont, Z., Kupiainen, K. and Höglund-Isaksson, L.: Scenarios of  
642 global anthropogenic emissions of air pollutants and methane until 2030, *Atmos. Environ.*, 41(38),  
643 8486–8499, doi:10.1016/j.atmosenv.2007.07.010, 2007.

644 Croci-Maspoli, M., Schwierz, C. and Davies, H. C.: Atmospheric blocking: space-time links to  
645 the NAO and PNA, *Clim. Dyn.*, 29(7-8), 713–725, doi:10.1007/s00382-007-0259-4, 2007.

646 Davini, P. and Cagnazzo, C.: On the misinterpretation of the North Atlantic Oscillation in  
647 CMIP5 models, *Clim. Dyn.*, 43(5-6), 1497–1511, doi:10.1007/s00382-013-1970-y, 2013.

648 Davini, P., Cagnazzo, C., Gualdi, S. and Navarra, A.: Bidimensional Diagnostics, Variability,  
649 and Trends of Northern Hemisphere Blocking, *J. Clim.*, 25(19), 6496–6509, doi:10.1175/JCLI-D-  
650 12-00032.1, 2012.

651 Eckhardt, S., Stohl, A., Beirle, S., Spichtinger, N., James, P., Forster, C., Junker, C., Wagner,  
652 T., Platt, U. and Jennings, S. G.: The North Atlantic Oscillation controls air pollution transport to  
653 the Arctic, *Atmos. Chem. Phys.*, 3(5), 1769–1778, doi:10.5194/acp-3-1769-2003, 2003.

654 EEA: European Environment Agency: Air quality in Europe, Tech. rep., Luxembourg,  
655 Publications Office of the European Union., 2013.

656 Feichter, J., Kjellström, E., Rodhe, H., Dentener, F., Lelieveld, J. and Roelofs, G.-J.:  
657 Simulation of the tropospheric sulfur cycle in a global climate model, *Atmos. Environ.*, 30(10-11),  
658 1693–1707, doi:10.1016/1352-2310(95)00394-0, 1996.

659 Feichter, J., Roeckner, E., Lohmann, U. and Liepert, B.: Nonlinear Aspects of the Climate  
660 Response to Greenhouse Gas and Aerosol Forcing, *J. Clim.*, 17(12), 2384–2398, doi:10.1175/1520-  
661 0442(2004)017<2384:NAOTCR>2.0.CO;2, 2004.

662 Fiore, A. M., Naik, V., Spracklen, D. V., Steiner, A., Unger, N., Prather, M., Bergmann, D.,  
663 Cameron-Smith, P. J., Cionni, I., Collins, W. J., Dalsøren, S., Eyring, V., Folberth, G. A., Ginoux,  
664 P., Horowitz, L. W., Josse, B., Lamarque, J.-F., MacKenzie, I. A., Nagashima, T., O’Connor, F. M.,  
665 Righi, M., Rumbold, S. T., Shindell, D. T., Skeie, R. B., Sudo, K., Szopa, S., Takemura, T. and  
666 Zeng, G.: Global air quality and climate., *Chem. Soc. Rev.*, 41(19), 6663–83,  
667 doi:10.1039/c2cs35095e, 2012.

668 Fischer-Bruns, I., Banse, D. F. and Feichter, J.: Future impact of anthropogenic sulfate aerosol  
669 on North Atlantic climate, *Clim. Dyn.*, 32(4), 511–524, doi:10.1007/s00382-008-0458-7, 2008.

670 Gillett, N. P. and Fyfe, J. C.: Annular mode changes in the CMIP5 simulations, *Geophys. Res.*  
671 *Lett.*, 40(6), 1189–1193, doi:10.1002/grl.50249, 2013.

672 Gleckler, P. J., Taylor, K. E. and Doutriaux, C.: Performance metrics for climate models, *J.*  
673 *Geophys. Res.*, 113(D6), D06104, doi:10.1029/2007JD008972, 2008.

674 Hilmer, M. and Jung, T.: Evidence for a recent change in the link between the North Atlantic  
675 Oscillation and Arctic Sea ice export, *Geophys. Res. Lett.*, 27(7), 989–992,  
676 doi:10.1029/1999GL010944, 2000.

677 Hoerling, M. P., Hurrell, J. W. and Xu, T.: Tropical origins for recent North Atlantic climate  
678 change., *Science*, 292(5514), 90–2, doi:10.1126/science.1058582, 2001.

679 Hori, M. E., Nohara, D. and Tanaka, H. L.: Influence of Arctic Oscillation towards the Northern  
680 Hemisphere Surface Temperature Variability under the Global Warming Scenario, *J. Meteorol. Soc.*  
681 *Japan*, 85(6), 847–859, doi:10.2151/jmsj.85.847, 2007.

682 Horton, D. E., Skinner, C. B., Singh, D. and Diffenbaugh, N. S.: Occurrence and persistence of  
683 future atmospheric stagnation events, *Nat. Clim. Chang.*, 4(8), 698–703, doi:10.1038/nclimate2272,  
684 2014.

685 Hu, Z.-Z. and Wu, Z.: The intensification and shift of the annual North Atlantic Oscillation in a  
686 global warming scenario simulation, *Tellus A*, 56(2), 112–124, doi:10.1111/j.1600-  
687 0870.2004.00050.x, 2004.

688 Hurrell, J. W.: Decadal trends in the north atlantic oscillation: regional temperatures and  
689 precipitation., *Science*, 269(5224), 676–9, doi:10.1126/science.269.5224.676, 1995.

690 IMAGE-team: The IMAGE 2.2 implementation of the SRES scenarios. A comprehensive  
691 analysis of emissions, climate change and impacts in the 21st century, CD-ROM Publ. Bilthoven,  
692 Natl. Inst. Public Heal. Environ., 2001.

693 IPCC: Climate Change 2013: The Physical Science Basis. Contribution of Working Group I to  
694 the Fifth Assessment Report of the Intergovernmental Panel on Climate Change, edited by T. F.  
695 Stocker, D. Qin, G.-K. Plattner, M. Tignor, S. K. Allen, J. Boschung, A. Nauels, Y. Xia, V. Bex,  
696 and P. M. Midgley, Cambridge University Press, Cambridge, United Kingdom and New York, NY,  
697 USA., 2013.

698 Jacob, D. J. and Winner, D. A.: Effect of Climate Change on Air Quality, *Atmos. Environ.*, 43,  
699 51–63 [online] Available from: <http://dash.harvard.edu/handle/1/3553961> (Accessed 9 October  
700 2014), 2009.

701 Karpechko, A. Y.: Uncertainties in future climate attributable to uncertainties in future  
702 Northern Annular Mode trend, *Geophys. Res. Lett.*, 37(20), L20702, doi:10.1029/2010GL044717,  
703 2010.

704 Kloster, S., Dentener, F., Feichter, J., Raes, F., van Aardenne, J., Roeckner, E., Lohmann, U.,  
705 Stier, P. and Swart, R.: Influence of future air pollution mitigation strategies on total aerosol  
706 radiative forcing, *Atmos. Chem. Phys.*, 8(21), 6405–6437, doi:10.5194/acp-8-6405-2008, 2008.

707 Kloster, S., Dentener, F., Feichter, J., Raes, F., Lohmann, U., Roeckner, E. and Fischer-Bruns,  
708 I.: A GCM study of future climate response to aerosol pollution reductions, *Clim. Dyn.*, 34(7-8),  
709 1177–1194, doi:10.1007/s00382-009-0573-0, 2009.

710 Kuzmina, S. I.: The North Atlantic Oscillation and greenhouse-gas forcing, *Geophys. Res.*  
711 *Lett.*, 32(4), L04703, doi:10.1029/2004GL021064, 2005.

712 Lim, G. H. and Wallace, J. M.: Structure and Evolution of Baroclinic Waves as Inferred from  
713 Regression Analysis, *J. Atmos. Sci.*, 48(15), 1718–1732, doi:10.1175/1520-  
714 0469(1991)048<1718:SAEOBW>2.0.CO;2, 1991.

715 Lohmann, U., Stier, P., Hoose, C., Ferrachat, S., Kloster, S., Roeckner, E. and Zhang, J.: Cloud  
716 microphysics and aerosol indirect effects in the global climate model ECHAM5-HAM, *Atmos.*  
717 *Chem. Phys.*, 7(13), 3425–3446, doi:10.5194/acp-7-3425-2007, 2007.

718 Müller, W. A. and Roeckner, E.: ENSO teleconnections in projections of future climate in  
719 ECHAM5/MPI-OM, *Clim. Dyn.*, 31(5), 533–549, doi:10.1007/s00382-007-0357-3, 2008.

720 Nakicenovic, N. and ...: Special Report on Emissions Scenarios: A Special Report of Working  
721 Group III of the Intergovernmental Panel on Climate Change, Cambridge University Press,  
722 Cambridge, UK., 2000.

723 Nazarenko, L. and Menon, S.: Varying trends in surface energy fluxes and associated climate  
724 between 1960 and 2002 based on transient climate simulations, *Geophys. Res. Lett.*, 32(22),  
725 L22704, doi:10.1029/2005GL024089, 2005.

726 Omrani, N.-E., Keenlyside, N. S., Bader, J. and Manzini, E.: Stratosphere key for wintertime  
727 atmospheric response to warm Atlantic decadal conditions, *Clim. Dyn.*, 42(3-4), 649–663,  
728 doi:10.1007/s00382-013-1860-3, 2013.

729 Pausata, F. S. R., Li, C., Wettstein, J. J., Nisancioglu, K. H. and Battisti, D. S.: Changes in  
730 atmospheric variability in a glacial climate and the impacts on proxy data: a model intercomparison,  
731 *Clim. Past*, 5, 489–502, doi:doi:10.5194/cp-5-489-2009, 2009.

732 Pausata, F. S. R., Pozzoli, L., Dingenen, R. Van, Vignati, E., Cavalli, F. and Dentener, F. J.:  
733 Impacts of changes in North Atlantic atmospheric circulation on particulate matter and human  
734 health in Europe, *Geophys. Res. Lett.*, 40(15), 4074–4080, doi:10.1002/grl.50720, 2013.

735 Pausata, F. S. R., Pozzoli, L., Vignati, E. and Dentener, F. J.: North Atlantic Oscillation and  
736 tropospheric ozone variability in Europe: model analysis and measurements intercomparison,  
737 *Atmos. Chem. Phys.*, 12(14), 6357–6376, doi:10.5194/acp-12-6357-2012, 2012.

738 Pelly, J. L. and Hoskins, B. J.: A New Perspective on Blocking, *J. Atmos. Sci.*, 60(5), 743–755,  
739 doi:10.1175/1520-0469(2003)060<0743:ANPOB>2.0.CO;2, 2003.

740 Peterson, K. A., Lu, J. and Greatbatch, R. J.: Evidence of nonlinear dynamics in the eastward  
741 shift of the NAO, *Geophys. Res. Lett.*, 30(2), 1030, doi:10.1029/2002GL015585, 2003.

742 Pham, M.: Changes in atmospheric sulfur burdens and concentrations and resulting radiative  
743 forcings under IPCC SRES emission scenarios for 1990–2100, *J. Geophys. Res.*, 110(D6), D06112,  
744 doi:10.1029/2004JD005125, 2005.

745 Rex, D. F.: Blocking Action in the Middle Troposphere and its Effect upon Regional Climate,  
746 *Tellus*, 2(3), 196–211, doi:10.1111/j.2153-3490.1950.tb00331.x, 1950.

747 Riahi, K. and Roehrl, R. A.: Greenhouse Gas Emissions in a Dynamics-as-Usual Scenario of  
748 Economic and Energy Development, *Technol. Forecast. Soc. Change*, 63(2-3), 175–205,  
749 doi:10.1016/S0040-1625(99)00111-0, 2000.

750 Roeckner, E., Bäuml, G., Bonaventura, L., Brokopf, R., Esch, M., Giorgetta, M., Hagemann, S.,  
751 Kirchner, I., Kornbluh, L., Manzini, E., Rhodin, A., Schlese, U., Schulzweida, U. and Tompkins,  
752 A.: The atmospheric general circulation model ECHAM5—Part I: Model description, *Tech. Rep.*  
753 349, Max-Planck-Institut für Meteorologie, Hamburg, Germany., 2003.

754 Roeckner, E., Bengtsson, L., Feichter, J., Lelieveld, J. and Rodhe, H.: Transient Climate  
755 Change Simulations with a Coupled Atmosphere–Ocean GCM Including the Tropospheric Sulfur  
756 Cycle, *J. Clim.*, 12(10), 3004–3032, doi:10.1175/1520-0442(1999)012<3004:TCCSWA>2.0.CO;2,  
757 1999.

758 Roeckner, E., Siebert, T. and Feichter, J.: Climatic response to anthropogenic sulfate forcing  
759 simulated with a general circulation model, in *Aerosol Forcing of Climate*, edited by R. J. Charlson  
760 and J. Heintzenberg, pp. 349–362, John Wiley & Sons Ltd., Chicester., 1995.

761 Roelofs, G.-J., Lelieveld, J. and Ganzeveld, L.: Simulation of global sulfate distribution and the  
762 influence on effective cloud drop radii with a coupled photochemistry sulfur cycle model, *Tellus B*,  
763 50(3), doi:10.3402/tellusb.v50i3.16098, 1998.

764 Rosenblatt, M.: Remarks on Some Nonparametric Estimates of a Density Function, *Ann. Math.*  
765 *Stat.*, 27(3), 832–837, 1956.

766 Scaife, A. A., Knight, J. R., Vallis, G. K. and Folland, C. K.: A stratospheric influence on the  
767 winter NAO and North Atlantic surface climate, *Geophys. Res. Lett.*, 32(18), L18715,  
768 doi:10.1029/2005GL023226, 2005.

769 Shindell, D., Kuylenstierna, J. C. I., Vignati, E., van Dingenen, R., Amann, M., Klimont, Z.,  
770 Anenberg, S. C., Muller, N., Janssens-Maenhout, G., Raes, F., Schwartz, J., Faluvegi, G., Pozzoli,  
771 L., Kupiainen, K., Höglund-Isaksson, L., Emberson, L., Streets, D., Ramanathan, V., Hicks, K.,  
772 Oanh, N. T. K., Milly, G., Williams, M., Demkine, V. and Fowler, D.: Simultaneously mitigating  
773 near-term climate change and improving human health and food security., *Science*, 335(6065), 183–  
774 9, doi:10.1126/science.1210026, 2012.

775 Sillmann, J., Pozzoli, L., Vignati, E., Kloster, S. and Feichter, J.: Aerosol effect on climate  
776 extremes in Europe under different future scenarios, *Geophys. Res. Lett.*, 40(10), 2290–2295,  
777 doi:10.1002/grl.50459, 2013.

778 Stephenson, D. B., Pavan, V., Collins, M., Junge, M. M. and Quadrelli, R.: North Atlantic  
779 Oscillation response to transient greenhouse gas forcing and the impact on European winter climate:  
780 a CMIP2 multi-model assessment, *Clim. Dyn.*, 27(4), 401–420, doi:10.1007/s00382-006-0140-x,  
781 2006.

782 Stier, P., Feichter, J., Kinne, S., Kloster, S., Vignati, E., Wilson, J., Ganzeveld, L., Tegen, I.,  
783 Werner, M., Balkanski, Y., Schulz, M., Boucher, O., Minikin, A. and Petzold, A.: The aerosol-  
784 climate model ECHAM5-HAM, *Atmos. Chem. Phys.*, 5(4), 1125–1156, doi:10.5194/acp-5-1125-  
785 2005, 2005.

786 Sundquist, H., Berge, E. and Kristjansson, J. E.: Condensation and cloud parameterization  
787 studies with a mesoscale numerical prediction model, *Mon. Wea. Rev.*, 117, 1641–1657, 1989.

788 Textor, C., Schulz, M., Guibert, S., Kinne, S., Balkanski, Y., Bauer, S., Bernsten, T., Berglen,  
789 T., Boucher, O., Chin, M., Dentener, F., Diehl, T., Feichter, J., Fillmore, D., Ginoux, P., Gong, S.,  
790 Grini, A., Hendricks, J., Horowitz, L., Huang, P., Isaksen, I. S. A., Iversen, T., Kloster, S., Koch,  
791 D., Kirkevåg, A., Kristjansson, J. E., Krol, M., Lauer, A., Lamarque, J. F., Liu, X., Montanaro, V.,  
792 Myhre, G., Penner, J. E., Pitari, G., Reddy, M. S., Seland, Ø., Stier, P., Takemura, T. and Tie, X.:  
793 The effect of harmonized emissions on aerosol properties in global models – an AeroCom  
794 experiment, *Atmos. Chem. Phys.*, 7(17), 4489–4501, doi:10.5194/acp-7-4489-2007, 2007.

795 Tibaldi, S. and Molteni, F.: On the operational predictability of blocking, *Tellus A*, 42(3), 343–  
796 365, doi:10.1034/j.1600-0870.1990.t01-2-00003.x, 1990.

797 Toon, O. B. and Ackerman, T. P.: Algorithms for the calculation of scattering by stratified  
798 spheres., *Appl. Opt.*, 20(20), 3657–60, doi:10.1364/AO.20.003657, 1981.

799 Twomey, S.: The Influence of Pollution on the Shortwave Albedo of Clouds, *J. Atmos. Sci.*,  
800 34(7), 1149–1152, 1977.

801 Vignati, E.: M7: An efficient size-resolved aerosol microphysics module for large-scale aerosol  
802 transport models, *J. Geophys. Res.*, 109(D22), D22202, doi:10.1029/2003JD004485, 2004.

803 Walker, G. T. and Bliss, E. W.: World weather V, *Mem. R. Meteorol. Soc.*, 4, 53 – 84, 1932.

804 WHO: Review of evidence on health aspects of air pollution – REVIHAAP Project. First  
805 results., Tech. rep., Copenhagen, World Health Organization., 2013.

806 Woollings, T., Hoskins, B., Blackburn, M. and Berrisford, P.: A New Rossby Wave–Breaking  
807 Interpretation of the North Atlantic Oscillation, *J. Atmos. Sci.*, 65(2), 609–626,  
808 doi:10.1175/2007JAS2347.1, 2008.

809 Yao, Y. and Luo, D.: Relationship between zonal position of the North Atlantic Oscillation and  
810 Euro-Atlantic blocking events and its possible effect on the weather over Europe, *Sci. China Earth  
811 Sci.*, doi:10.1007/s11430-014-4949-6, 2014.

812 Yiou, P. and Nogaj, M.: Extreme climatic events and weather regimes over the North Atlantic:  
813 When and where?, *Geophys. Res. Lett.*, 31(7), L07202, doi:10.1029/2003GL019119, 2004.

814  
815

816 **Table 1:** ECHAM5-HAM experiment design and number of years simulated for each experiment.  
 817 The original denomination used by Kloster et al. (2009) is shown in the last column.

Experiment	GHG	Aerosol emissions	Years of simulation	Original names
2000	2000	2000	60	CONTROL
2030	2030	2030	30	GHG+AE
2030GHG	2030	2000	30	GHG
2030AER	2000	2030	30	AE

818  
 819 **Table 2:** Skewness values for the PM distributions of the four selected regions for each  
 820 experiment. For each region and experiment, changes relative to all the other experiments are  
 821 significant at the 95% confidence level, except for 2030-2030AER in Western Mediterranean.

	Western Mediterranean	Eastern Mediterranean	Central Europe	Eastern Europe
2000	0.26	0.83	1.44	1.70
2030	1.02	0.95	0.66	1.18
2030GHG	0.48	1.26	1.18	1.08
2030AER	1.05	1.17	0.94	1.03

822  
 823 **Table 3:** *PM relative anomalies (unitless) associated to different percentiles for the WM and*  
 824 *CE regions in the 2000 experiment (first and third rows) and their relative changes (in %)* for  
 825 the 2030 simulation compared to 2000 values (second and fourth rows).

Region	Experiment	Percentile				
		5 <sup>th</sup>	25 <sup>th</sup>	50 <sup>th</sup>	75 <sup>th</sup>	95 <sup>th</sup>
Western Mediterranean	2000	0.49	0.73	1.01	1.25	1.57
	2030	+8%	+1%	-9%	-7%	+4%
Central Europe	2000	0.65	0.80	0.94	1.13	1.48
	2030	-14%	-3%	+2%	+2%	+7%

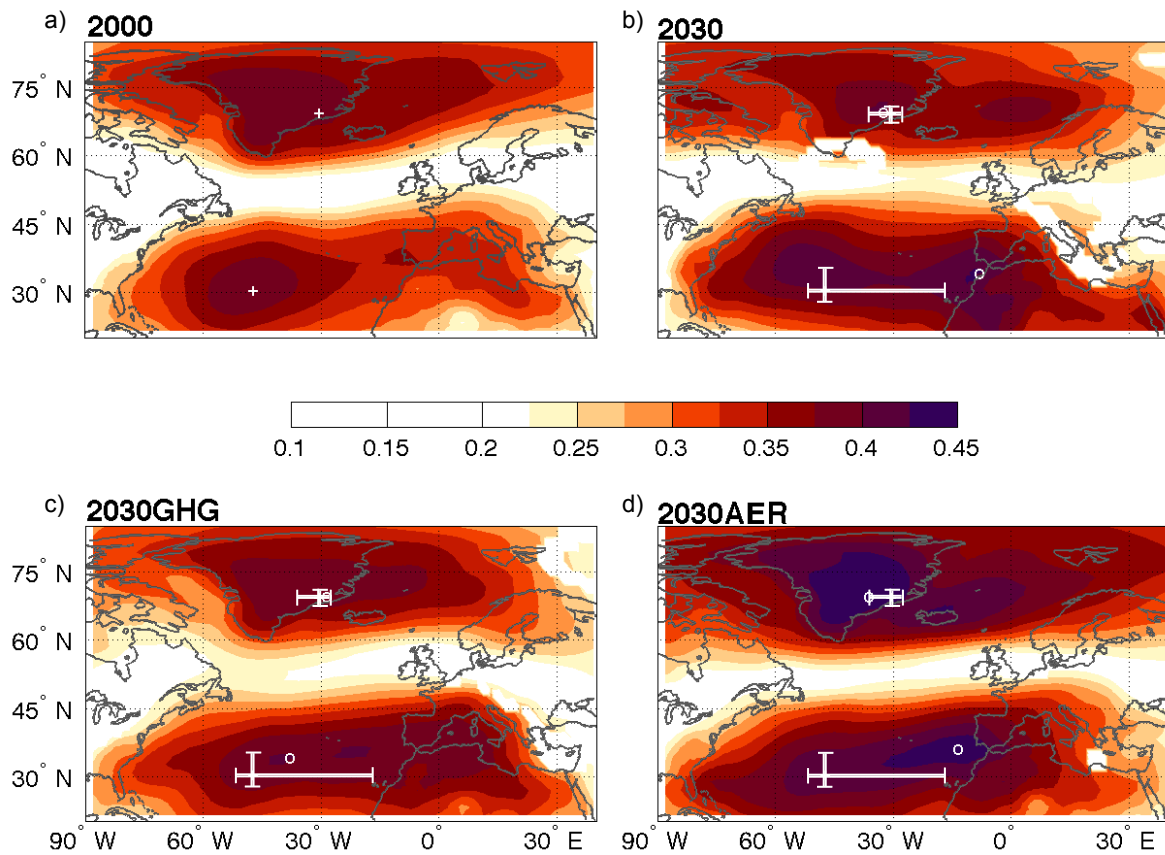
826  
 827 **Table 4:** Qualitative contributions (small (+), medium (++) , high (+++)) of 2030 GHG and AER to  
 828 changes in the NAO phase, SCOA location and blocking event frequency. For the blocking events  
 829 the direction of the increased frequency is also shown. The contributions significant at 95%  
 830 confidence level are shown in bold

	Impact on NAO	Impact on SCOA	Impact on Blocking Events
2030GHG	++	+	<b>North ++</b> <b>East +</b>
2030AER	+	<b>+++</b>	<b>North ++</b> <b>East +++</b>
2030 (GHG+AER)	<b>+++</b>	<b>+++</b>	<b>North +++</b> <b>East +++</b>



832

833



834

835

836

837

838

839

840

841

842

843

844

845

846

847

848

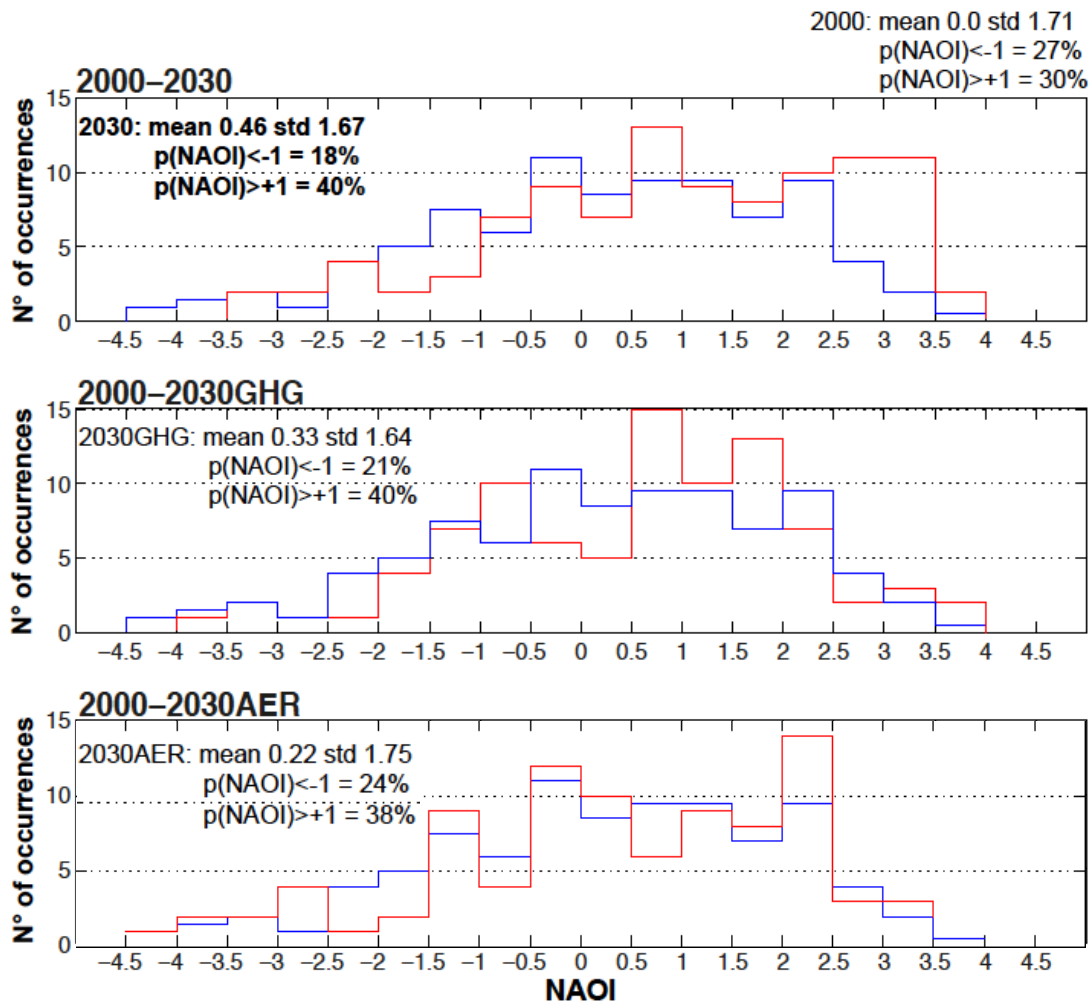
849

850

**Fig. 1:** Sea Level Pressure coherence index maps of the North Atlantic sector for the 2000 (a) and 2030 (b) simulations and the two sensitivity studies (c and d) in winter (DJF). The SLP centres of action (COAs) for the control run and for the 2030 simulations are shown by white crosses and white circles, respectively. The bars delimit the range between the 10<sup>th</sup> and 90<sup>th</sup> percentile of the CI maxima in the 2000 simulations. Only areas in which the difference between the 2000 control pattern and the sensitivity simulation is significant at the 95% confidence level and CI values are greater than 0.225 are shaded. The choice of shading only CI values greater than 0.225 is arbitrary.

851

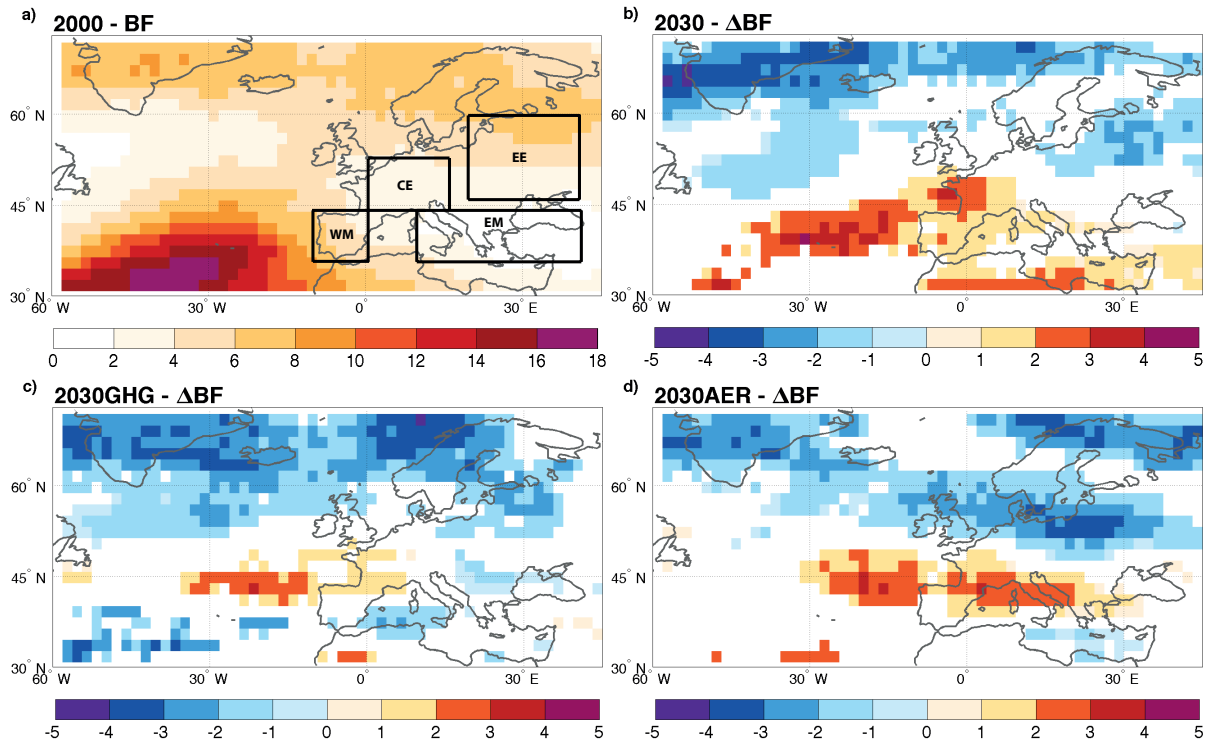
852



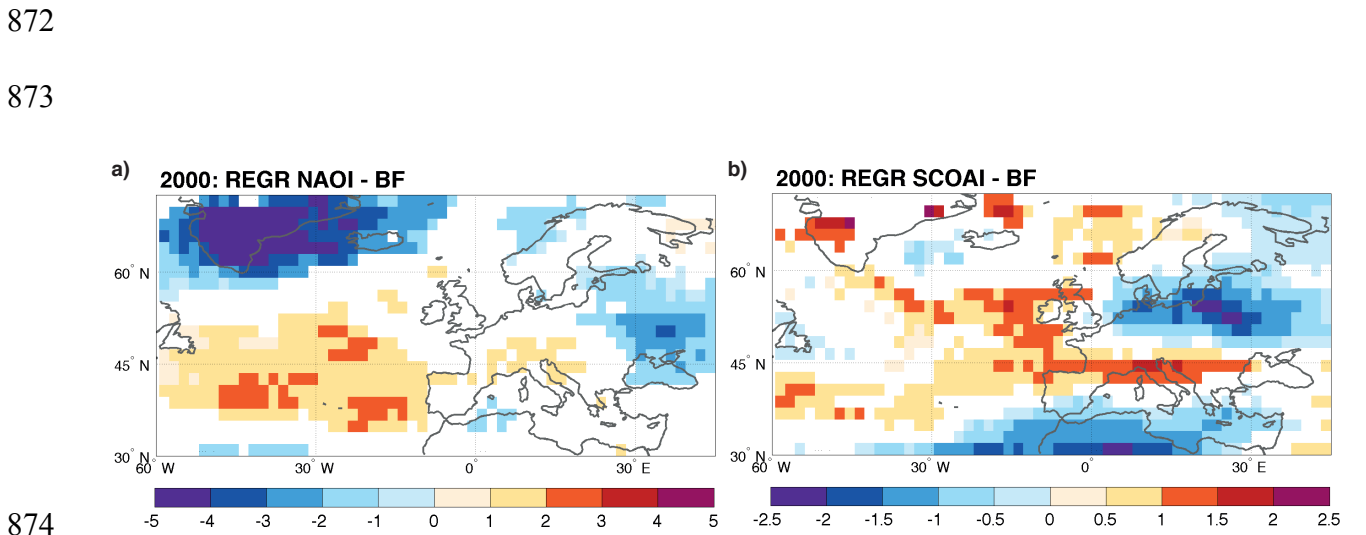
853

854 **Fig. 2:** Frequency distributions of the winter (DJF) NAOI for the 2000 control simulation (blue,  
855 all panels), 2030 (red, upper panel), 2030GHG (red, central panel) and 2030AER (red, lower  
856 panel). Numbers show the NAOI mean value, the standard deviation (std) and the probability of  
857 having a NAOI greater than +1 ( $p(\text{NAOI}) > +1$ ) or smaller than -1 ( $p(\text{NAOI}) < -1$ ). Values of the  
858 simulations having a NAOI mean significantly different from 2000 control mean at 95%  
859 confidence level are shown in bold. The 2000s mean NAO is by definition equal to 0 and the  
860 number of occurrences has been normalized to 30 years for a direct comparison with the other  
861 simulations.

862

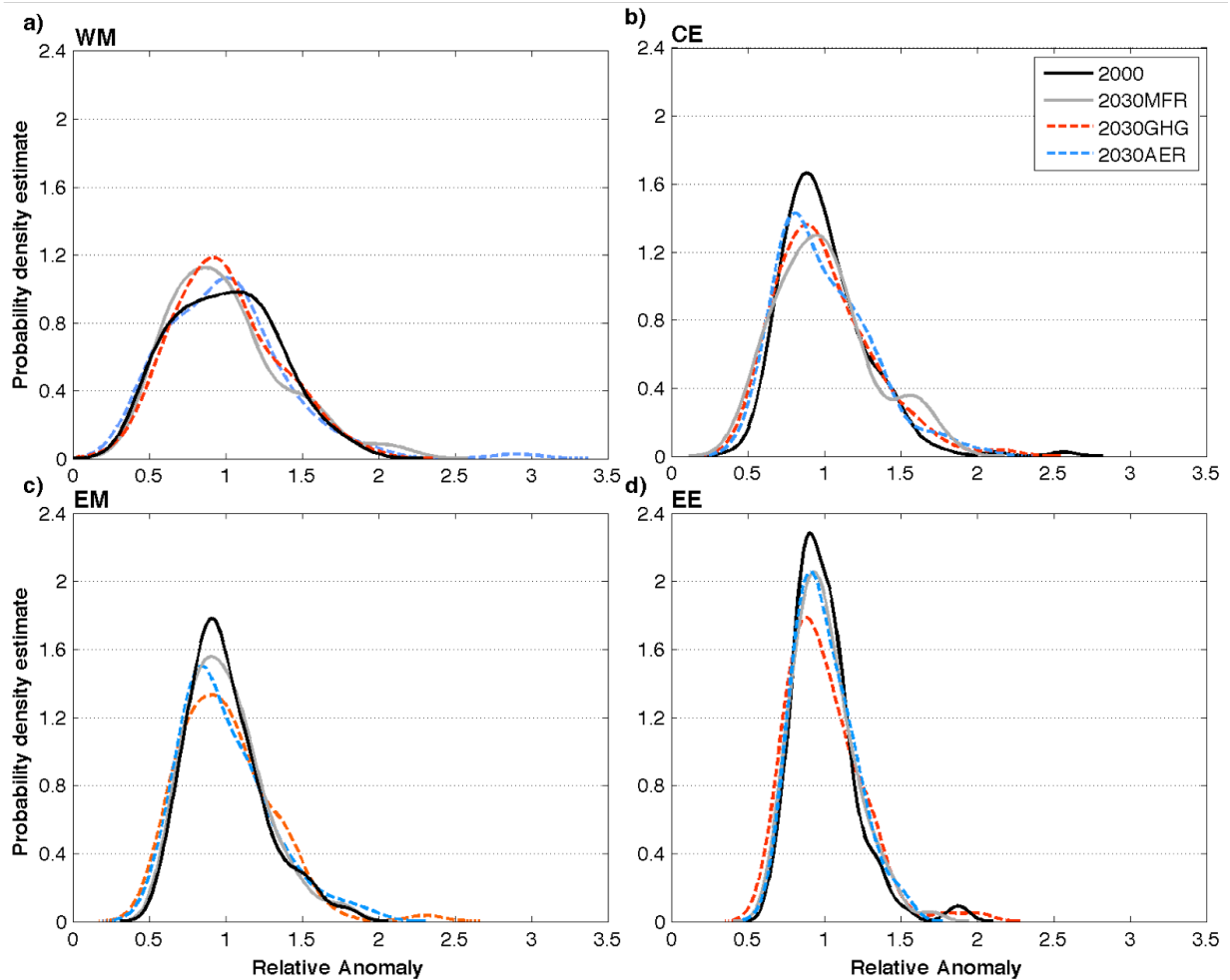


865  
 866 **Fig. 3:** Blocking frequency (in % of days in which a blocking event occurs at a given grid box)  
 867 over the Atlantic sector for the 2000 simulation (a); changes in blocking frequency compared to  
 868 the 2000 simulation for 2030 (b), 2030GHG (c) and 2030AER (d) simulations in winter (DJF).  
 869 Only areas in which the difference between the 2000 control and the sensitivity simulation is  
 870 significant at 95% confidence level are shaded (in white non-significant areas). In panel (a) we  
 871 have highlighted the regions discussed in Section 3.3 and Table 2.



874  
 875 **Fig. 4:** Blocking frequency anomalies (in % of days in which a blocking event occur at a given  
 876 grid box) per unit of NAOI index (NAOI, a) and SCOAI index (SCOAI, b) standard deviation.  
 877 The anomalies are calculated using a one-point regression analysis (see Appendix B). Only  
 878 differences significant at the 95% confidence level are shown (based on the correlation  
 879 significance between NAOI/SCOAI and blocking frequency). Note that the two panels use  
 880 different colour-scales.

881  
882  
883  
884



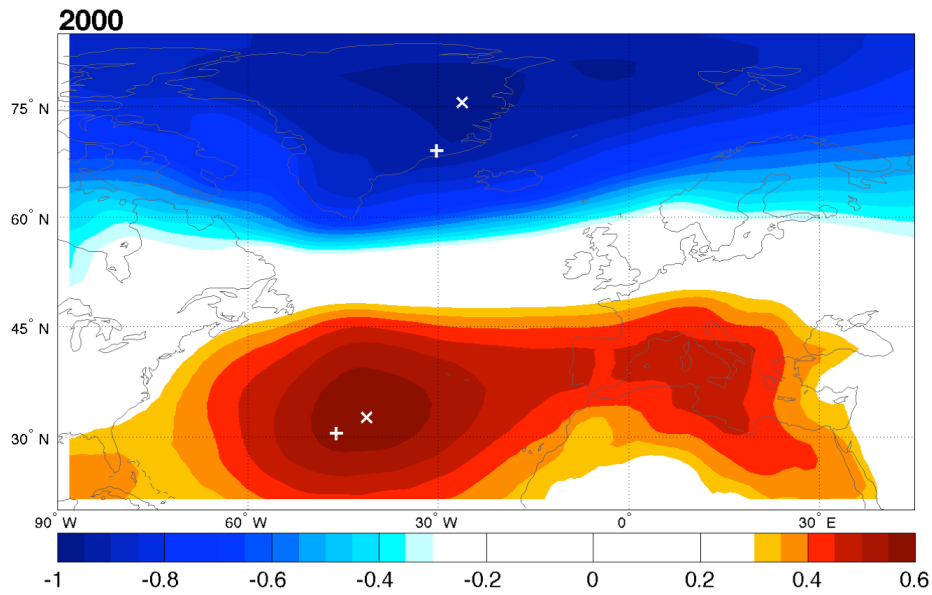
885

886 **Fig. 5:** Probability density estimate (PDE) of PM relative anomalies for each region (Western  
887 and Eastern Mediterranean, Central and Eastern Europe) and for each experiment. Relative  
888 anomalies are computed as the ratio between winter (DJF) monthly timeseries and the winter  
889 (DJF) climatology of each experiment and region. The probability density estimates are based on  
890 a normal kernel function, which provides non-parametric PDEs for random variables  
891 (Rosenblatt, 1956). The probability for a given relative anomaly to occur is obtained by  
892 integrating the PDE in  $dx$ .

893  
894  
895  
896

897

898



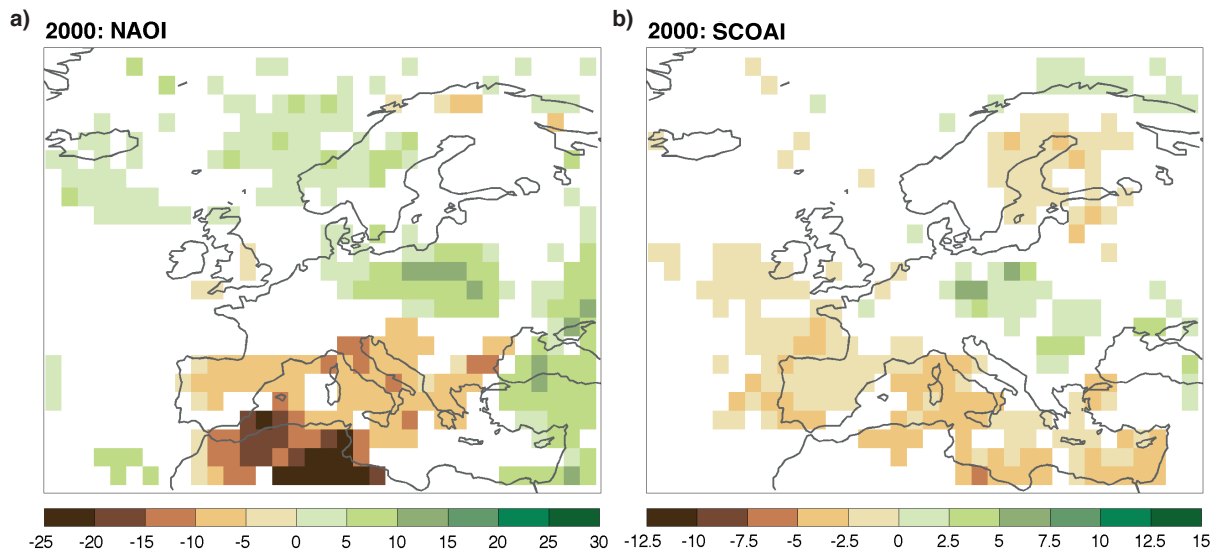
899

900

901

902

**Figure A1:** Correlations between North Atlantic winter SLP (December to February) and the PC1 of SLP. The markers indicate the maxima in CI (+ sign) and in the SLP/PC1 (x sign) correlations.



903

904

905

906

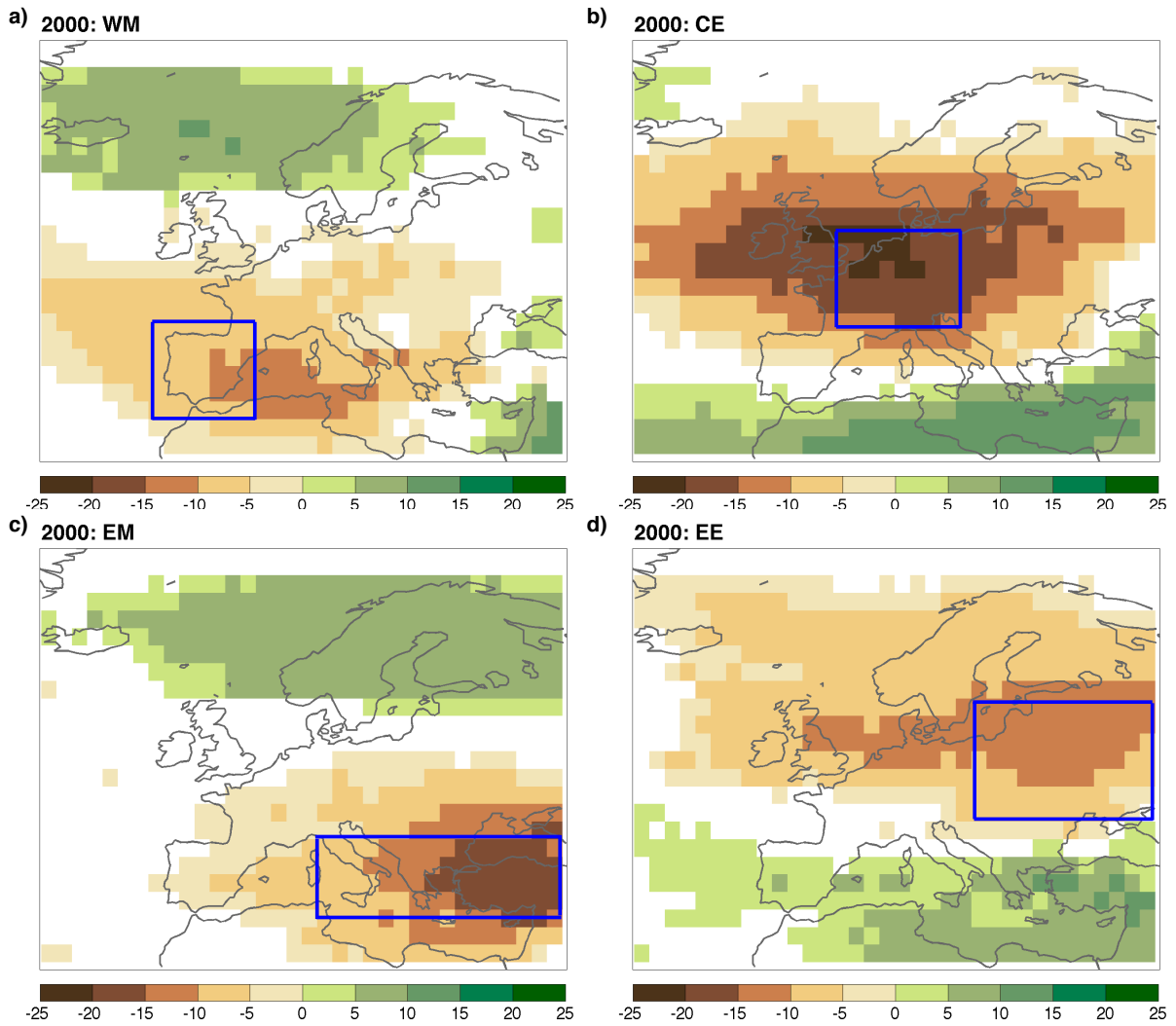
907

908

909

910

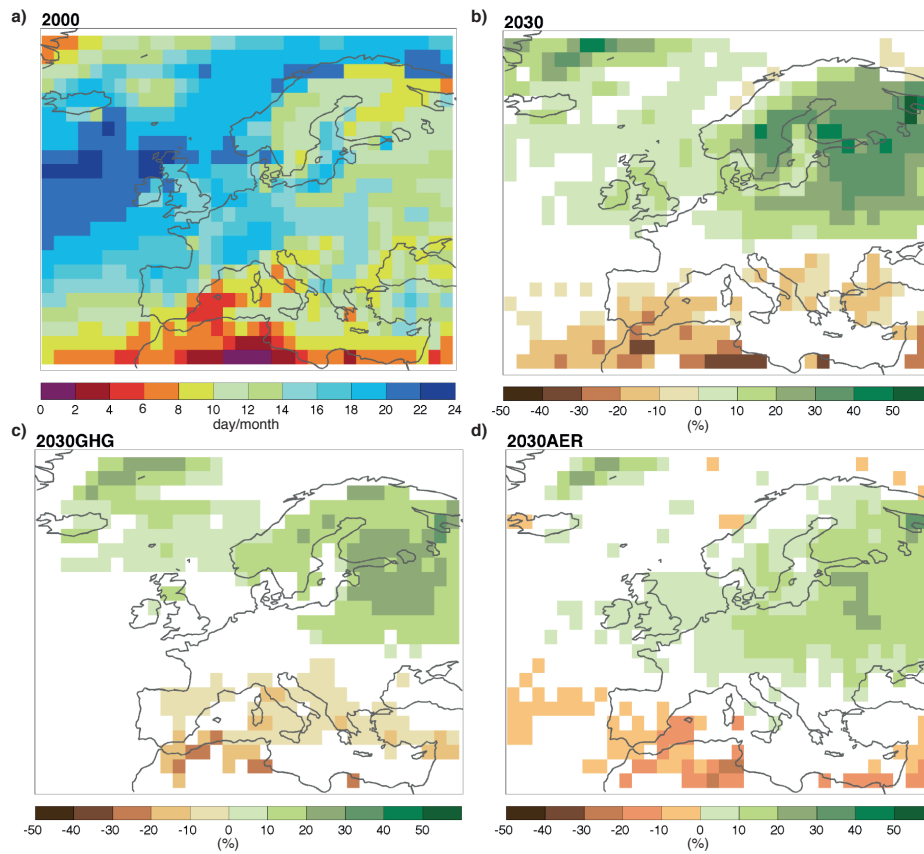
**Fig. B1:** Rainy day anomalies (in %) per unit of NAOI (a) and CI time-series (b) standard deviation. The CI time-series has been constructed as described in Appendix B. The anomalies are calculated using a one-point regression analysis. Only differences significant at the 95% confidence level are shown. Note that the two panels use different colour-scales.



911

912 **Fig. B2:** The values at each gridpoint show the composite anomaly in rainy days (in %) in the  
 913 selected domain – a) WM, b) CE, c) EM, d) EE) – while said gridpoint is blocked relative to  
 914 rainy days in the selected domain while the gridpoint is unblocked. The composite is taken by  
 915 averaging the rainy day anomaly maps obtained for each gridbox within the selected domain. For  
 916 example, in panel a) (WM) the positive values over southern Norway indicate that, when there is  
 917 a blocking event there, rainy days over the WM increase by about 10% compared to the case  
 918 with no blocking over southern Norway. On the other hand, blocking events west and over the  
 919 WM lead to 10-15% precipitation anomalies relative to the case with no blocking events over the  
 920 same regions. The regional domains analysed in each panel are marked by the blue rectangles.

921



922

923 **Fig. C1:** Average number of rainy day per month during winter (DJF) in the 2000 simulation (a).  
 924 Percent changes in the average number of rainy days per month for 2030 (b), 2030GHG (c), and  
 925 2030AER (d) simulations during winter. Only differences significant at the 95% confidence level  
 926 are shown.

927